Alternating hemiplegia of childhood associated mutations in Atp1a3 reveal diverse neurological alterations in mice

Terrey, M.; Krivoshein, G.; Adamson, S.I.; Arystarkhova, E.; Anderson, L.; Szwec, J.; ... ; Lutz, C.M.

Neurobiology of Disease 212 (2025) 106954

Contents lists available at ScienceDirect

Neurobiology of Disease

journal homepage: www.elsevier.com/locate/ynbdi

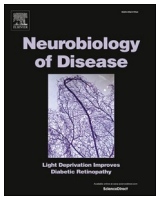

Alternating hemiplegia of childhood associated mutations in *Atp1a3* reveal diverse neurological alterations in mice

Markus Terrey [a], Georgii Krivoshein [b,c], Scott I. Adamson [d], Elena Arystarkhova [e,f], Laura Anderson [a], John Szwec [a], Shelby McKee [a], Holly Jones [a], Sara Perkins [a], Vijay Selvam [a], Pierre-Alexandre Piec [a], Dweet Chhaya [a], Ari Dehn [a], Aamir Zuberi [g], Stephen A. Murray [a,h,i], Natalia S. Morsci [j], Kathleen J. Sweadner [e,f], David A. Knowles [d,k], Else A. Tolner [b,c], Arn M.J.M. van den Maagdenberg [b,c], Cathleen M. Lutz [a,i,*]

[a] *Rare Disease Translational Center, The Jackson Laboratory, Bar Harbor, ME, USA*
[b] *Department of Human Genetics, Leiden University Medical Centre, Leiden, Netherlands*
[c] *Department of Neurology, Leiden University Medical Centre, Leiden, Netherlands*
[d] *New York Genome Center, New York, NY, USA*
[e] *Department of Neurosurgery, Massachusetts General Hospital, Boston, MA, USA*
[f] *Harvard Medical School, Boston, MA, USA*
[g] *Technology Evaluation and Development, The Jackson Laboratory, Bar Harbor, ME, USA*
[h] *Genetic Resource Science, The Jackson Laboratory, Bar Harbor, ME, USA*
[i] *JAX Center for Precision Genetics, The Jackson Laboratory, Bar Harbor, ME, USA*
[j] *Hope for Annabel, Washington, DC, USA*
[k] *Department of Computer Science and Department of Systems Biology, Columbia, New York, NY, USA*

ARTICLE INFO

Keywords:
AHC
ATP1A3
Dystonia
Seizure
ATPase activity
Spreading depolarization
And Neuroinflammation

ABSTRACT

Pathogenic variants in the neuronal Na^+/K^+ ATPase transmembrane ion transporter (*ATP1A3*) cause a spectrum of neurological disorders including alternating hemiplegia of childhood (AHC). The most common *de novo* pathogenic variants in AHC are p.D801N (~40 % of patients) and p.E815K (~25 % of patients), which lead to early mortality by spontaneous death in mice. Nevertheless, knowledge of the development of clinically relevant neurological phenotypes without the obstacle of premature death, is critical for the identification of pathophysiological mechanisms and ultimately, for the testing of therapeutic strategies in disease models. Here, we used hybrid vigor attempting to mitigate the fragility of AHC mice and then performed behavioral, electrophysiological, biochemical, and molecular testing to comparatively analyze mice that carry either of the two most common AHC patient observed variants in the *Atp1a3* gene. Collectively, our data reveal the presence but also the differential impact of the p.D801N and p.E815K variants on disease relevant alterations such as spontaneous and stress-induced paroxysmal episodes, motor function, behavioral and neurophysiological activity, and neuroinflammation. Our alternate AHC mouse models with their phenotypic deficits open novel avenues for the investigation of disease biology and therapeutic testing for ATP1A3 research.

1. Introduction

ATP1A3 encodes the neuronal Na^+/K^+ ATPase transmembrane ion transporter necessary to regulate neuronal excitability. Familial and more commonly *de novo* heterozygous variants in *ATP1A3* cause multiple syndromes including alternating hemiplegia of childhood (AHC), rapid-onset dystonia parkinsonism (RDP), and cerebellar ataxia, pes cavus, optic atrophy, and sensorineural hearing loss (CAPOS) with nearly non-overlapping pathogenic variants (Haq et al., 2019; Heinzen et al., 2014; Panagiotakaki et al., 2010; Salles et al., 2021; Tranebjærg et al., 2018). Although pathogenic variants in *ATP1A3* have been linked to various syndromes (e.g., AHC, RDP, CAPOS), patients also exhibit common manifestations such as dystonia, seizures, ataxia, and cognitive impairment, indicating the possibility of shared disease mechanisms

* Corresponding author at: Rare Disease Translational Center, The Jackson Laboratory, Bar Harbor, ME, USA.
E-mail address: Cat.Lutz@jax.org (C.M. Lutz).

https://doi.org/10.1016/j.nbd.2025.106954
Received 8 January 2025; Received in revised form 8 May 2025; Accepted 9 May 2025
Available online 15 May 2025

(Boonsimma et al., 2020; Ishii et al., 2013; Li et al., 2022; Panagiotakaki et al., 2015; Pavone et al., 2022b; Rosewich et al., 2012; Salles et al., 2021; Viollet et al., 2015).

Over 1000 individuals with pathogenic variants in *ATP1A3* have been identified, of which ~70 % are diagnosed with AHC (Li et al., 2022; Vezyroglou et al., 2022). The most common heterozygous *de novo* missense AHC variants are p.D801N (~40 %), p.E815K (~25 %) and p.G947R (~10 %) that concentrate within or near the transmembrane domains of the ATP1A3 protein (Heinzen et al., 2014; Li et al., 2022; Vezyroglou et al., 2022). AHC patients are affected by sudden and spontaneous episodes (paroxysmal spells), which may be a combination of different symptoms such as hemiplegia, dystonia and seizures. Psychological (e.g., excitement, anxiety, anticipation, fright) and environmental stressors (e.g., temperature changes, water exposure) may trigger paroxysmal episodes in AHC patients (Heinzen et al., 2014; Salles et al., 2021). Children and adolescents suffer from the loss of mobility, epilepsies, and complications such as aspiration that can result in early death (Moya-Mendez et al., 2021; Pavone et al., 2022a, 2022b; Salles et al., 2021). Dystonia refers to recurrent episodes of sustained muscle contraction that leads to twisting, repetitive movements or abnormal posture (Van Der Heijden et al., 2022). In general, dystonia is considered a complex neuropathological condition of the motor system involving numerous neuronal circuits of the brain including those of the basal ganglia, thalamus, cortex, brainstem, and cerebellum (Aïssa et al., 2022; Hallett, 2011; Jinnah et al., 2017; Loher and Krauss, 2009; Neychev et al., 2008). Adding to the complexity is the presence of seizures (e.g., focal and generalized seizures), which also underly elaborate neuronal networks (Chauhan et al., 2022; Mueller et al., 2019; Wu et al., 2018). Despite the biological complexity, efforts continue trying to delineate the etiology, involvement of specific brain circuits, and potential long-term consequences that may occur with age and/or because of repetitive paroxysmal episodes in AHC (e.g., neurological regression and deterioration) (Perulli et al., 2022; Saito et al., 2010; Uchitel et al., 2021).

The Na^+/K^+ ATPase is a heterotrimeric α-β-FXYD protein complex with one of the four α isoforms (α1–4) that are encoded by the *ATP1A1–4* genes (Heinzen et al., 2014; Palmgren and Nissen, 2011). The α1 subunit is almost ubiquitously expressed while expression of α2 is restricted (e.g., skeletal, cardiac, and vascular muscle, glia cells, adipose tissues), and α4 subunit expression is observed in male germ cells (Holm et al., 2016; McGrail et al., 1991; Syeda et al., 2020). Expression of the α3 isoform (*ATP1A3*) is observed in excitatory and inhibitory neurons of the mammalian central nervous system including the cortex, hippocampus, striatum, cerebellum, and brainstem (Allen Brain Atlas, Human Protein Atlas, brainrnaseq.org) (Dobretsov et al., 2019; Gokce et al., 2016; Jiao et al., 2022; Smith et al., 2021). In addition, lower ATP1A3 expression has also been observed in the human heart but not in all other species (MGI gene expression data, EMBL single cell expression atlas) (Henriksen et al., 2013; Herrera et al., 1994; McLellan et al., 2020; Premont et al., 2022; Shamraj et al., 1991; Sweadner et al., 1994).

ATP1A3 is critical in restoring the transient increase in intracellular Na^+ concentration after repeated action potentials and in supporting neurotransmitter re-uptake, and thereby, determines the electrical excitability of neurons (Azarias et al., 2013; Dobretsov et al., 2019; Holm et al., 2016; Holm and Lykke-Hartmann, 2016; Zou et al., 2023). Homozygosity for either patient-observed variants or loss of ATP1A3 (*Atp1a3* $^{-/-}$) cause death shortly after birth in mice (Clapcote et al., 2009; Holm et al., 2016; Ikeda et al., 2013). Moreover, heterozygous loss of ATP1A3 (*Atp1a3* $^{+/-}$) is tolerated in mice without the development of gross morphological, behavioral, dystonia, and survival defects, but causes hyperactivity and enhanced motor locomotion (DeAndrade et al., 2011; Ikeda et al., 2013; Liu et al., 2024; Moseley et al., 2007). In stark contrast, mice that are heterozygous for AHC patient associated variants such as p.D801N and p.E815K (referred to as AHC mice) exhibit motor dysfunction, and develop spontaneous and severe stress-induced paroxysmal episodes (Heinzen et al., 2014; Helseth et al., 2018; Hunanyan et al., 2014; Ng et al., 2021; Salles et al., 2021). Interestingly, AHC variants cause reduced ATPase activity, inhibit ATP1A3 pump current, and disturb neuronal excitability. Together with the severe deficits observed in AHC mice, this suggests a potentially dominant-negative disease mechanism for AHC causing variants (Arystarkhova et al., 2019; Heinzen et al., 2012; Li et al., 2015; Simmons et al., 2018; Sweadner et al., 2019).

Several pathogenic AHC variants have been introduced in mice (Clapcote et al., 2009; Hawkins et al., 2024; Helseth et al., 2018; Holm et al., 2016; Hunanyan et al., 2014; Isaksen et al., 2017). The most common p.D801N and p.E815K mutations are associated with early postnatal mortality in mice, and this complicates their experimental investigation. We speculated that hybrid vigor may be sufficient to manage the observed fragility of AHC mouse models. In the presence of hybrid vigor, survival defects were delayed in AHC mice, which allowed us to analyze and directly compare *in vivo* deficits mediated by the D801N and E815K mutations in mice.

2. Results

2.1. Hybrid vigor prevents early mortality without abolishing the development of spontaneous and stress-induced paroxysmal spells in B6C3 AHC mice

The two most common dominant *de novo* variants in AHC are p.D801N and p.E815K. The corresponding heterozygous D801N ('Mashlool' mouse model; *Atp1a3* ^{tm1Ute}) and E815K ('Matoub' mouse model; *Atp1a3* $^{tm1.1Mika}$) animal AHC models have been previously generated and maintained on a congenic C57BL/6J (B6J) background (Helseth et al., 2018; Hunanyan et al., 2014; Uchitel et al., 2021). In addition to the 'Mashlool' mouse model, we also introduced the patient-observed D801N variant in C57BL/6J mice (C57BL/6J-*Atp1a3*^{em3Lutzy}/Lutzy, Materials and Methods, Liu et al., 2024). The B6J D801N and E815K mouse models are highly valuable for ATP1A3 research because mice develop spontaneous and stress-induced paroxysmal spells, which are reminiscent of those observed in patients (Helseth et al., 2018; Hunanyan et al., 2014). Notably, spontaneous death starts after birth and the majority of mutant mice fail to survive past 12 weeks of age (Helseth et al., 2018; Hunanyan et al., 2021; Liu et al., 2024). Unfortunately, routine (e.g., breeding, weaning, cage changes) and experimental handling of mice can already induce lethal events (Helseth et al., 2018; Hunanyan et al., 2014), which challenges the ability to maintain a stable and effective 'live colony' for either pathogenic variant in B6J mice.

In contrast to pure inbred strains, hybrid vigor allows mice to regain genetic heterozygosity and thereby are more often resistant to stress and survive better (Birchler et al., 2006; Chan et al., 2017; Linder and Davission, 2004; Selman and Swindell, 2018). Intentionally introducing genetic diversity to mitigate limitations that may arise from inbreeding is a common solution in mouse husbandry, and numerous inbred strains e.g., DBA, C3H, CBA and CAST are viable options for crossing. In the context of seizure traits, C3H (C3H/HeJ) mice are perhaps particularly interesting because their seizure response greatly differs from that of B6J mice or other inbred strains for various seizure paradigms (Mouse Phenome Database), which led to the discovery of C3H harboring multiple susceptibility and seizure modifier genes (Beyer et al., 2008; Frankel et al., 2014; Tokuda et al., 2009). For example, a benefit of C3H has been observed for other mouse models including Alzheimer mouse models (e.g. APP/PS1 mouse model), which suffer from seizures and mortality when maintained on a congenic B6J background while those defects are absent on a hybrid C3H background (Carlson et al., 1997; Jankowsky et al., 2004; Minkeviciene et al., 2009). Consequently, these animal models are available on either genetic background at public strain repositories.

In an attempt to overcome limitations caused by the fragility and/or early lethality of the B6J AHC mouse models, we crossed the pathogenic B6J D801N and E815K variants onto a C3H hybrid background (referred

to as 'B6C3', Materials and Methods) to generate B6C3.*Atp1a3* $^{D801N/+}$ (B6C3 D801N) and B6C3.*Atp1a3* $^{E815K/+}$ (B6C3 E815K) mice. While deaths on a B6J background start after birth with ~50 % of mutant mice failing to even reach wean age (~postnatal day P28) (Hunanyan et al., 2021; Liu et al., 2024), hybrid B6C3 D801N and E815K mice showed a noticeable onset of unexpected deaths at ~8 and ~15 weeks of age, respectively (Fig. 1A and B). Mortality of B6C3.*Atp1a3* $^{D801N/+}$ and B6C3.*Atp1a3* $^{E815K/+}$ males was generally higher compared to that of mutant female mice (Fig. 1A and B). While death of B6C3.*Atp1a3* $^{D801N/+}$ mice was sudden and spontaneous, only ~50 % of the recorded deaths of B6C3.*Atp1a3* $^{E815K/+}$ mice were spontaneous (both sexes). The remaining proportion of deaths of B6C3.*Atp1a3* $^{E815K/+}$ mice required humane euthanasia as a study end point ('death') as mice reached an alarmingly low body condition score (BCS) and body weight, even more so than B6C3.*Atp1a3* $^{D801N/+}$ mice (Fig. S1A and B).

The ATP1A1 (α1), ATP1A2 (α2) and ATP1A3 (α3) subunits contribute to the total enzymatic Na^+/K^+-ATPase activity in the nervous system. We utilized hippocampal tissue samples to assess the ATPase activity in B6C3 AHC mice. The total enzymatic Na^+/K^+-ATPase activity was reduced by ~39 % in both B6C3 AHC mice (Fig. 1C). The introduction of either the D801N or E815K mutation did not affect the levels of ATP1A3 (α3) expression (Fig. S1C and D). In rodents, the α1 subunit is much less sensitive to the inhibition by ouabain than α2 and α3, and was used to separately assess the activity due to α1 (Price and Lingrel, 1988). The α2 + α3 ATPase activity was reduced by ~43 % in B6C3.*Atp1a3* $^{D801N/+}$ and ~ 47 % in B6C3.*Atp1a3* $^{E815K/+}$ mice (Fig. 1C). The remaining activity of ~55 % in B6C3 AHC mice comprises the ATPase activity that should derive from the unaffected wild type ATP1A3 (α3) subunit and that of the less abundant glial specific α2 subunit. In contrast, the ATPase activity conferred by the ATP1A1 (α1) subunit that is more ouabain-resistant compared to ATP1A3 (α3) and ATP1A2 (α2) was not affected by either AHC mutation (Fig. 1C). These data suggest a near complete impairment in the α3 ATPase activity specific to that of the mutant ATP1A3 protein in both B6C3 D801N and E815K mice, which is consistent with previous *in vitro* studies (Heinzen et al., 2012; Weigand et al., 2014).

Patients with AHC suffer from spontaneous spells of symptoms (e.g. dystonia, hemiplegia, and seizures), and B6J AHC mice seem to exhibit similar defects (Helseth et al., 2018; Hunanyan et al., 2014). Handling of mutant mice may be sufficient to induce and observe episodes, which could perhaps, underlie the sudden and spontaneous death in B6J AHC mice (Helseth et al., 2018; Hunanyan et al., 2014). However, we did not witness spontaneous paroxysmal events merely during the routine handling of B6C3 AHC mice. Aiming to better understand the unexpected death of B6C3.*Atp1a3* $^{D801N/+}$ and B6C3.*Atp1a3* $^{E815K/+}$ mice, we housed naïve mice in the DIVA (Digital In Vivo Alliance) cage system from ~13–22 weeks of age, which enables continuous video-monitoring of animal activity in their home cage without any operator or experimental interference. We observed that B6C3.*Atp1a3* $^{D801N/+}$ mice (N = 7) showed a rapid burst in activity including running, jumping and climbing up the wall, just prior to a lethal event that was characterized by freezing, tail and limb twisting, twitching and extension (Supplementary file 1). B6C3.*Atp1a3* $^{E815K/+}$ mice (N = 11) appeared overtly lethargic just prior to their sudden death (Supplementary file 2). Nine of the B6C3.*Atp1a3* $^{E815K/+}$ mice had an observable episode of freezing and limb twitching (Supplementary file 2) while the remaining mutant mice rather collapsed, which did not allow us to confidently visualize a behavioral episode of freezing and twisting. Although challenged by the fact that the recordings reflect time frames of multiple weeks, we still wondered whether mice would experience multiple spontaneous episodes. Manually inspecting the recordings, we found at least two instances for B6C3.*Atp1a3* $^{D801N/+}$ (N = 2) and one for B6C3.*Atp1a3* $^{E815K/+}$ (N = 1) mice in which mutant mice had an episode, appeared to recover, and later died because of another episode.

While paroxysmal episodes may not have a clear trigger; stress, exercise, excitement, extreme heat or cold, water exposure, or changes in lighting have been identified to cause episodes in patients with AHC (Heinzen et al., 2014; Salles et al., 2021). Therefore, multiple conditions to experimentally evoke paroxysmal spells have been previously tested, and hypothermia has been identified as a robust trigger in *Atp1a3* mutant mice (Isaksen et al., 2017; Uchitel et al., 2021). To investigate whether B6C3 AHC mice are also susceptible to this stressor, we adopted the previously described hypothermia paradigm (Fig. S1E, Materials and Methods) (Isaksen et al., 2017; Pizoli et al., 2002). Mice were placed in 5 °C cold water to abruptly induce hypothermia with a body temperature reduction of ~10 °C (Fig. S1F). As expected (Hunanyan et al., 2021; Isaksen et al., 2017), no paroxysmal episodes were observed in wild type mice (Fig. 1D). In contrast, hypothermic B6C3.*Atp1a3* $^{D801N/+}$ mice consistently developed paroxysmal episodes with severe dystonia-like postures, lack of voluntary movement, and hyperextended, cramped and stiffened extremities (e.g., legs, paws and/or tail) during the recovery period (Fig. 1D, examples shown in Fig. S1G, Materials and Methods). In agreement with previous hypothermia studies (Hunanyan et al., 2021; Isaksen et al., 2017), spontaneous bursts of 'convulsion-like' movements were also observed in B6C3.*Atp1a3* $^{D801N/+}$ mice (Fig. 1E, Supplementary file 3), suggesting that mice may experience a combination of symptoms similar to AHC patients. B6C3.*Atp1a3* $^{E815K/+}$ mice also developed paroxysmal episodes with dystonia-like postures but had a significantly greater range in severity with a few of the B6C3.*Atp1a3* $^{E815K/+}$ mice even failing to show any abnormal behavior (Fig. 1D, Fig. S1G). In addition, no 'convulsion-like' events were observed in these 'non-responding' B6C3.*Atp1a3* $^{E815K/+}$ mice (Fig. 1E). Previous studies noted that the penetrance of paroxysmal spells may be ~50 % or more in hypothermic B6J D801N (dystonia- and convulsion-like events) and ~ 65 % in forced swim tested B6J E815K mice (dystonia- but no convulsion-like events, water temperature of 40 °C) (Helseth et al., 2018; Hunanyan et al., 2021). Importantly, hypothermic B6C3.*Atp1a3* $^{D801N/+}$ (complete penetrance) and hypothermic B6C3.*Atp1a3* $^{E815K/+}$ (~90 % penetrance) mice developed paroxysmal episodes characterized by dystonia- and convulsion-like body postures, highlighting that these clinically relevant deficits are robust in our hybrid vigor B6C3 AHC models.

Furthermore, paroxysmal spells severely impaired voluntary movement and mobility of B6C3 AHC mice and concordantly, mutant mice had a significant delay until regaining movement control and returning to normal behavior compared to wild type mice (Fig. 1F and G). In addition to the data shown (Fig. 1F and G), we initially worked with B6C3.*Atp1a3* $^{D801N/+}$ mice (> 50 mice) to establish and validate the hypothermia protocol. Collectively, less than 3 % of AHC mice failed to recover during testing and instead died because of apparently lethal hypothermia-induced paroxysmal spells. B6C3 AHC mice also showed a delay in body temperature recovery (Fig. S1F). Although we cannot rule out a link between paroxysmal spells and thermoregulation in mutant mice, we speculate that the delay in body temperature recovery may rather be influenced by the lower body weight of the mutant mice (Fig. S1A and B).

2.2. *B6C3 AHC mice exhibit impaired motor function and altered behavioral activity*

Adding to the dysfunction of the motor system that is evident by the development of dystonia, AHC patients also suffer from ataxia and that in turn, impedes their ability to balance, stand, walk, and run. During routine handling, we noticed that B6C3.*Atp1a3* $^{E815K/+}$ mice developed an unsteady gait, and it became visually notable at ~12 weeks of age (Supplementary file 4). Therefore, we subjected B6C3 AHC mice to rotarod testing to assess their motor function. B6C3.*Atp1a3* $^{D801N/+}$ and B6C3.*Atp1a3* $^{E815K/+}$ mice showed reduced rotarod performance compared to that of wild type mice, further supporting the impairment of motor function in both B6C3 AHC models (Fig. 2A). Interestingly, B6C3.*Atp1a3* $^{D801N/+}$ mice retained better rotarod performance with age compared to B6C3.*Atp1a3* $^{E815K/+}$ mice (Fig. 2A). Motor performance

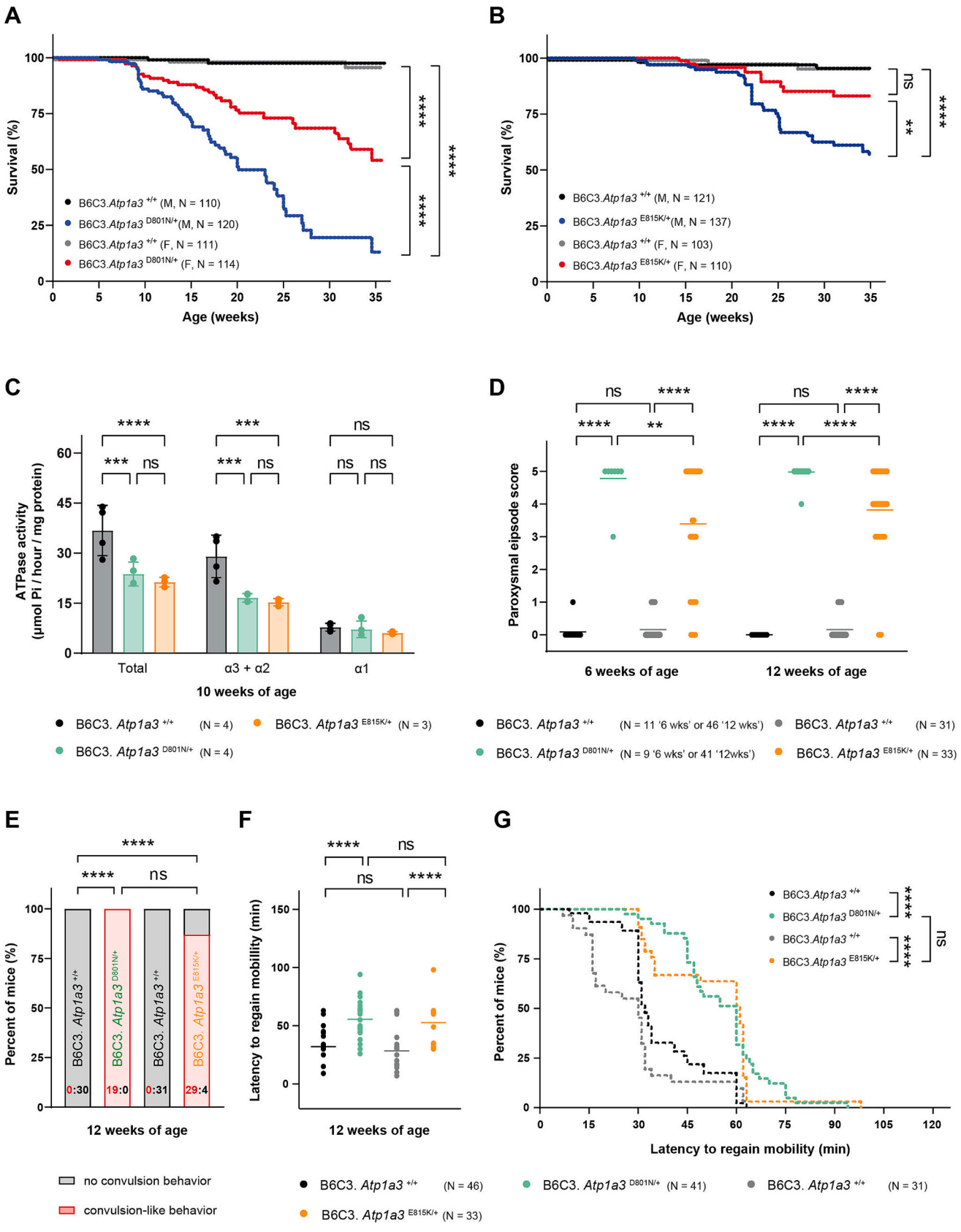

(caption on next page)

Fig. 1. B6C3 AHC mice develop spontaneous and stress-induced paroxysmal spells. (A) Kaplan-Meier survival curve of B6C3.*Atp1a3* $^{D801N/+}$ mice. Wild type littermate controls are shown (black and grey). (B) Kaplan-Meier survival curve of B6C3.*Atp1a3* $^{E815K/+}$ mice. Approximately 50 % of B6C3.*Atp1a3* $^{E815K/+}$ mice required euthanasia as the study end point ('death') due to the low body condition score (BCS). Spontaneous and BCS required deaths are included in the survival curve. Wild type littermate controls are shown (black and grey). (C) Analysis of the ATPase activity of tissues from the hippocampus of B6C3.*Atp1a3* $^{D801N/+}$ and B6C3.*Atp1a3* $^{E815K/+}$ mice. The data represent the mean ± SD. (D) Hypothermia induced paroxysmal spells (HIP) were induced in B6C3.*Atp1a3* $^{D801N/+}$ and B6C3.*Atp1a3* $^{E815K/+}$ mice. Dystonia-like events were scored during the recovery period of HIP experiments and the horizontal line (mean) for each group represents the average score. Wild type littermate controls for each mutant strain are shown (black and grey). (E) The occurrence of convulsive-like events of B6C3 AHC mice. The data are shown as the fraction (percent) of mice without (grey) or with (red) convulsion-like defects that were observed during the recovery period of HIP experiments. The exact number of mice without (black font) and with (red font) convulsion-like defects is shown in each bar. Wild type littermate controls for each mutant strain are shown. (F) Latency to regain mobility and movement control is shown. The horizontal line for each group represents the mean. Wild type littermate controls for each mutant strain are shown (black and grey). (G) The data in F are shown as a Kaplan-Meier curve. Wild type littermate controls for each mutant strain are shown (black and grey). M, males; F, females; BCS, body condition score. Mantel-Cox test (A, B, G); Two-way ANOVA was corrected for multiple comparisons using Tukey method (C, D); Fisher's exact test (E); One-way ANOVA was corrected for multiple comparisons using Tukey method (F). ns, not significant; ** $p \leq 0.01$; *** $p \leq 0.001$; **** $p \leq 0.0001$. See also Fig. S1. (For interpretation of the references to colour in this figure legend, the reader is referred to the web version of this article.)

not only reflects baseline motor activity but also motor learning ('modification of motor activity'), which occurs as a result of 'practicing' and internal changes in the motor networks (Baladron et al., 2023; Cording and Bateup, 2023; Kogan et al., 2023; Seidler, 2010). Gross motor activity (baseline) and motor learning can be simultaneously or selectively affected (Cording and Bateup, 2023; Duchon et al., 2011; Levin et al., 2006; Pass et al., 2022; Verslegers et al., 2015; Vo et al., 2018; Wagner et al., 2019). While wild type mice improved their rotarod performance over consecutive testing days as expected, neither B6C3.*Atp1a3* $^{D801N/+}$ nor B6C3.*Atp1a3* $^{E815K/+}$ mice improved their performance, indicating that motor learning is also impaired in these mice (Fig. S2A).

Intrigued by the improved survival, motor system deficits, and the ability to handle B6C3 AHC mice and because mild-to-moderate social and cognitive impairments have been observed in patients with AHC (Pavone et al., 2022a, 2022b; Polanowska et al., 2018; Uchitel et al., 2020), we investigated whether additional behavioral alterations can be detected in B6C3 AHC mice. We assessed the grip strength of B6C3.*Atp1a3* $^{D801N/+}$ and B6C3.*Atp1a3* $^{E815K/+}$ mice. While B6C3 AHC mouse models exhibited a reduction in grip strength, no grip defects were observed when normalized to the body weight of mice (Fig. S2B).

Moreover, naïve B6C3.*Atp1a3* $^{D801N/+}$ and B6C3.*Atp1a3* $^{E815K/+}$ mice were subjected to open field testing, which assesses changes as a function of exploratory and/or locomotor activity since mice are allowed to freely navigate within a novel environment (Carter and Shieh, 2015; Seibenhener and Wooten, 2015; Tatem et al., 2014). B6C3.*Atp1a3* $^{E815K/+}$ mice showed a significant increase in the total distance traveled while B6C3.*Atp1a3* $^{D801N/+}$ mice showed a notably greater range in the distance traveled, which was only significantly increased when not correcting for multiple comparison (Fig. 2B). Furthermore, B6C3.*Atp1a3* $^{E815K/+}$ mice also showed an increase in the movement time and correspondingly, a decrease in the rest time (Fig. 2C and D). In addition, the number of stereotypic episodes, which typically reflect repetitive behavioral patterns (e.g., head bobbing, grooming), was also increased in B6C3.*Atp1a3* $^{E815K/+}$ mice (Fig. 2E). In contrast, the movement time, rest time and stereotypic episodes of B6C3.*Atp1a3* $^{D801N/+}$ were comparable to wild type mice (Fig. 2C, D and E). While B6C3.*Atp1a3* $^{E815K/+}$ mice showed changes in horizontal activity (e.g., movement and rest time), we observed a reduction in vertical activity (rearing) of B6C3.*Atp1a3* $^{D801N/+}$ mice (Fig. 2F). However, neither B6C3.*Atp1a3* $^{D801N/+}$ nor B6C3.*Atp1a3* $^{E815K/+}$ mice exhibited significant differences in the time spent in the center or the outer zone (margin) of the open field arena, in which changes could be indicative of anxiety-related behaviors (Fig 2G). Although activity changes in the open field arena can be impacted and correlated with physical and/or locomotor deficits (e.g., ataxia, tremor, muscle weakness); the directionality of the observed activity changes in D801N (reduction in vertical activity) and E815K (increase in horizontal activity) mice failed to tie in with the motor, body weight and grip strength deficits (Fig. 2A, Fig. S1A and B, and Fig. S2B). Alternatively, the differential changes in open field activity may instead reflect functional changes in exploratory (e.g., cognitive) behavior of B6C3 AHC mice.

Some patients with AHC and *ATP1A3*-related syndromes show bradycardia and cardiac rhythm abnormalities (e.g., shortened QTc intervals) (Balestrini et al., 2020; Jaffer et al., 2015; Moya-Mendez et al., 2021). Pathogenic variants in *ATP1A3* may directly or indirectly impair heart function through the excessive excitability of the brain (Aiba and Noebels, 2015; Balestrini et al., 2020; Hunanyan et al., 2014). However, no significant electrocardiogram changes (e.g., interval and amplitude) were observed in B6C3 AHC mice (Fig. S2C).

2.3. B6C3 AHC mice exhibit altered hippocampal and cortical network activity

Patients with AHC, especially those with the pathogenic p.E815K variant, may develop severe seizures and epilepsy (Capuano et al., 2020; Ford et al., 2023; Panagiotakaki et al., 2015; Viollet et al., 2015). Previous electrophysiological recordings in hippocampal slices of B6J AHC mice revealed an increase in neuronal excitability, which may contribute to the observed seizure susceptibility in patients (Clapcote et al., 2009; Hunanyan et al., 2018). Using cortical (visual cortex, V1 and motor cortex, M1) and hippocampal (dorsal CA1 area) alternating current local field potential (AC-LFP) and direct current (DC)-potential recordings in freely behaving wild type, B6C3. *Atp1a3* $^{D801N/+}$, and B6C3.*Atp1a3* $^{E815K/+}$ mice (Fig. 3A), we searched for possible epileptiform activities and other alterations in neuronal activity in the brain of B6C3 AHC mice at various ages (e.g., AC-LFP trace examples at 14 weeks of age, Fig. 3B). Consistent with the influence of the C3H genetic background (Frankel et al., 2014), spike-wave discharges (SWD) were observed in the M1 cortex of B6C3 wild type mice but were much less frequent in B6C3 AHC mice (Fig. 3C). The rate of hippocampal spikes increased in B6C3.*Atp1a3* $^{E815K/+}$ mice with age up to ~65 spikes/h at 14 weeks of age (Fig. 3D), while in B6C3.*Atp1a3* $^{D801N/+}$ the rate was similar to that in wild type mice and remained constantly low over the different ages (Fig. 3D). Furthermore, only B6C3.*Atp1a3* $^{E815K/+}$ mice showed hippocampo-cortical giant spikes that are epileptiform features predictive of seizures (Gureviciene et al., 2019), and the rate of giant spikes increased with age up to ~6 giant spikes/h at 14 weeks of age (Fig. 3E).

In addition to the spiking activities, we observed rare events in the cortical and hippocampal DC-potential recordings that are characterized as spreading depolarizations (SD). In B6C3.*Atp1a3* $^{D801N/+}$ mice a single spontaneous SD event was identified at 6 weeks of age that was first observed in motor (M1) cortex and then appeared in visual (V1) cortex, without appearing in the dorsal hippocampus (dHC) even though the LFP signal was also suppressed in this brain structure (Fig. S3A). The SD event was preceded by a burst of spiking activity in M1 cortex (Fig. S3B). In contrast, ~50 % of B6C3.*Atp1a3* $^{E815K/+}$ mice exhibited spontaneous SD events (example traces in Fig. S3C, E and G). The SDs were consistently first observed in hippocampus (99 % bilaterally) and with a small

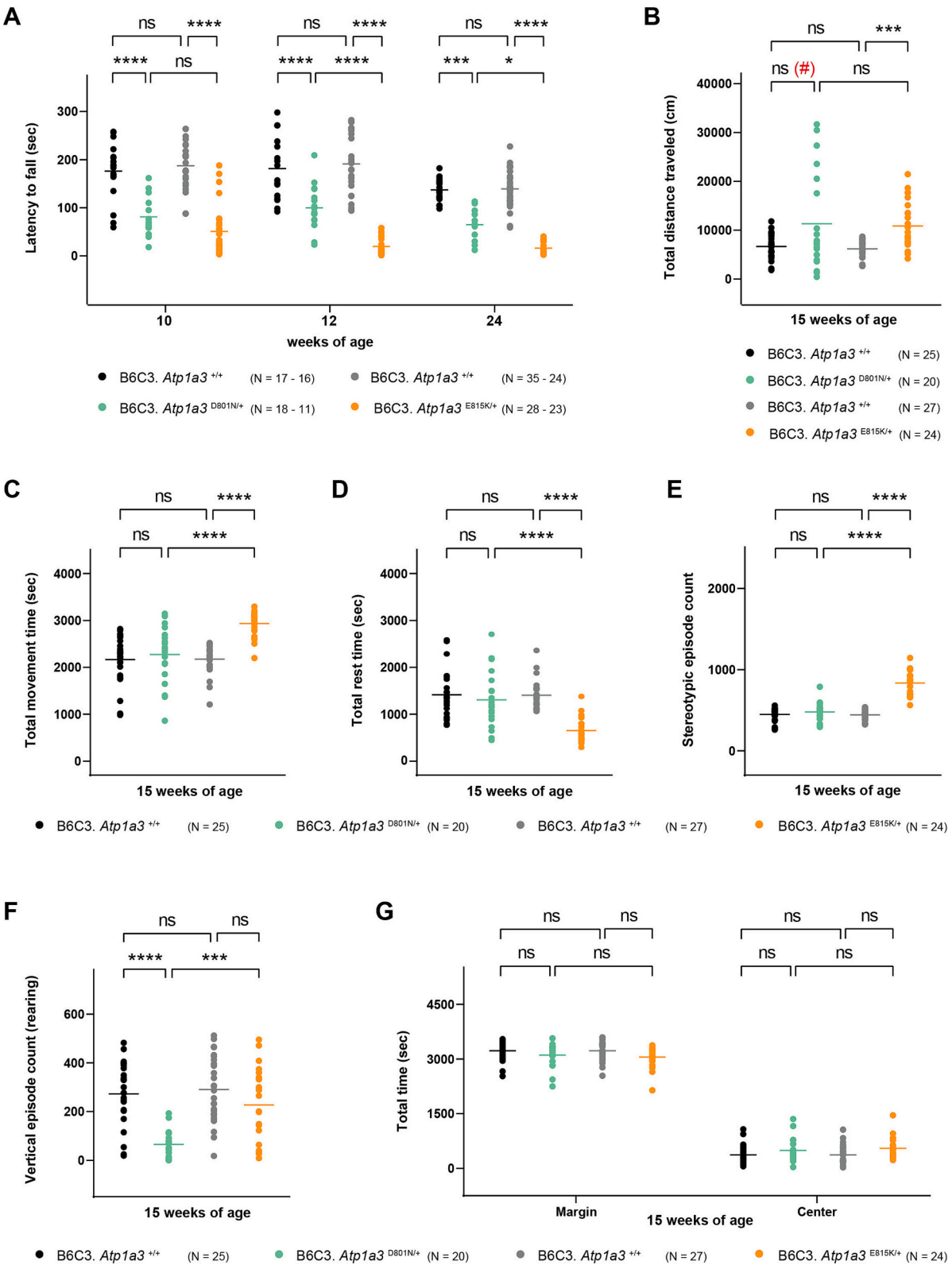

Fig. 2. B6C3 AHC mice show motor and behavioral deficits. (A) Latency of B6C3 AHC mice to fall off the accelerating rotarod at various ages. The horizontal line for each group represents the mean. Wild type littermate controls for each mutant strain are shown (black and grey). (B) to (G) Naïve B6C3 AHC mice were subjected to open field testing to interrogate exploratory and/or locomotor activity. The horizontal line for each group represents the mean. Wild type littermate controls for each mutant strain are shown (black and grey). (B) Total distance traveled. Note: # D801N mice only showed a "significant" difference in total distance traveled when the data were not corrected for multiple comparisons. p = value of 0.0051 compared to littermate control mice (black) or p = value of 0.0018 when compared to wild type mice (grey). (C) Total movement time. (D) Total rest time. (E) Stereotypic episodes. (F) Vertical episodes. (G) Total time spent in the center or margin of the open field arena. Two-way ANOVA was corrected for multiple comparisons using Tukey method (A, G); One-way ANOVA was corrected for multiple comparisons using Tukey method (B, C, D, E, F). ns, not significant; * $p \leq 0.05$; *** $p \leq 0.001$; **** $p \leq 0.0001$. See also Fig. S2.

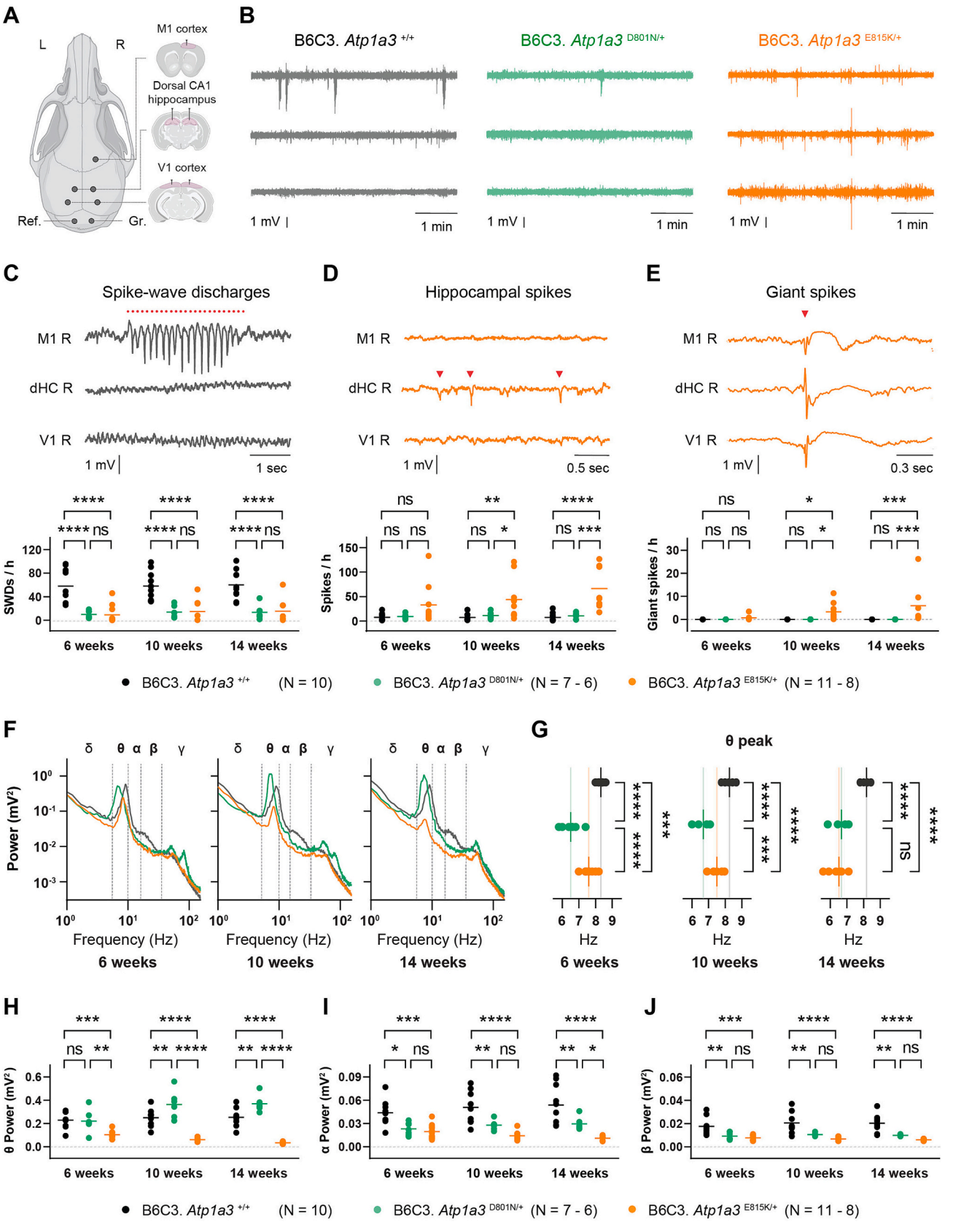

(caption on next page)

Fig. 3. B6C3 AHC mice show altered hippocampal and cortical network activity. (A) Schematic representation of LFP recording electrodes placed in motor (M1) and visual (V1) cortex and dorsal CA1 hippocampus. Recordings were performed for 3 consecutive days per time point. Electrodes for reference (Ref.) and ground (Gr.) were placed in cerebellum. (B) Example traces of 5-min AC-LFP traces from the M1, dorsal CA1 hippocampus, and V1 (top-to-bottom) of wild type (black), B6C3.*Atp1a3* $^{D801N/+}$ (green) and B6C3.*Atp1a3* $^{E815K/+}$ (orange) mice at 14 weeks of age. (C) Example trace of spike-wave discharge (SWD) event in frontal M1 cortical channel recorded in wild type mice at 14 weeks of age. SWDs present as a prominent burst (highlighted by the red dotted line) of negative polarity spikes and a positive polarity wave, exclusively seen in the frontal M1 cortical channel with no corresponding activity in V1 cortical or dHC channels. The horizontal line for each group represents the average SWD frequency per hour. (D) Example traces of hippocampal spike events (red arrowheads) in the dorsal CA1 hippocampus of B6C3.*Atp1a3* $^{E815K/+}$ mice at 14 weeks of age. These concerned isolated hippocampal spikes that were not observed in M1 and V1 cortices. The horizontal line for each group represents the average spike frequency per hour. (E) Example traces of hippocampo-cortical giant spike observed in B6C3.*Atp1a3* $^{E815K/+}$ mice. A giant spike consists of a simultaneous large spike of varying polarity (indicated by the red arrowhead) seen in all channels that is followed by a slow negative-positive potential shift lasting >0.3 s in the M1 cortical channel and accompanied by a slow positive deflection lasting up to 600 ms in dHC and V1 cortex. The horizontal line for each group represents the average giant spike frequency per hour. (F) Average V1 cortical power spectral densities (PSD) during active wakefulness of wild type (black), B6C3.*Atp1a3* $^{D801N/+}$ (green) and B6C3.*Atp1a3* $^{E815K/+}$ (orange) mice. (G) Leftward shift of θ frequency peak observed in B6C3 AHC mice from 6 weeks onward. The vertical line for each group represents the mean. (H) Absolute power at θ frequency from the V1 cortical PSD during active wakefulness. The horizontal line for each group represents the mean. (I) Absolute power at α frequency from the V1 cortical PSD during active wakefulness. The horizontal line for each group represents the mean. (J) Absolute power at β frequency from the V1 cortical PSD during active wakefulness. The horizontal line for each group represents the mean. Ref, reference electrode; Gr, ground electrode; M1, motor cortex; V1, visual cortex; dHC, dorsal hippocampus CA1; CA1, hippocampal cornu ammonis area 1; SWD, spike-wave discharge. Two-way ANOVA was corrected for multiple comparisons using Tukey method (C, D, E, H, I, J); One-way ANOVA was corrected for multiple comparisons using Tukey method (G). ns, not significant; * $p \leq 0.05$; ** $p \leq 0.01$; *** $p \leq 0.001$; **** $p \leq 0.0001$. The depicted top view of the mouse skull with electrode configuration and coronal brain views were created using BioRender.com (A). See also Figs. S3 and S4. (For interpretation of the references to colour in this figure legend, the reader is referred to the web version of this article.)

delay also appeared in cortex (Fig. S3C and E). The likelihood that hippocampal SDs also appeared in cortex increased with age (20 % of SDs at 10 weeks; 54 % of SDs at 14 weeks). When appearing in cortex, SD events were first observed in the V1 cortex (43 % unilateral and 57 % bilateral) and from there propagated in a caudal-to-rostral pattern to M1 cortex in 85 % of SD events (Fig. S3E). Hippocampal SDs in B6C3.*Atp1a3* $^{E815K/+}$ mice were preceded by an epileptiform burst (Racine scale score 1–3) (Racine, 1972) that was characterized by high-amplitude spikes in hippocampal LFP synchronous with lower-amplitude spikes in cortical LFP (Fig. S3D and F). The duration of the hippocampal burst activity preceding the SDs was not different for SDs that did or did not appear in cortex (Fig. S3H). However, SD events with the appearance in the cortex exhibited higher burst spiking frequency as well as prolonged time to 50 % SD recovery and a higher amplitude in hippocampus (Fig. S3H).

To get a more detailed perspective of the brain activity changes, visual cortex AC-LFP recordings were used to analyze the power spectral density (PSD). The PSD from mouse LFP can be categorized into five frequency bands (i.e., δ (1–5 Hz), θ (5–10 Hz), α (10–13 Hz), β (13–30 Hz), and γ (30–100 Hz) bands) (Fig. S4A), which in animals and humans are associated with various neurological activities and behaviors and when altered may provide insight in disease mechanisms (Drinkenburg et al., 2015; Tivadar and Murray, 2019). We first focused on the θ band because changes could be indicative of abnormal cognitive and motor function as well as epilepsy (Jansen et al., 2021; Kropotov, 2009; Luo et al., 2024; Perez et al., 2024; Tan et al., 2024). During periods of active wakefulness, characterized by faster frequencies of brain activity and high levels of θ activity (V1 cortical LFP example in Fig. S4B), PSD analysis revealed a leftward shift in the θ frequency peak in both B6C3 AHC mice (Fig. 3F and G). While the θ frequency peak in B6C3.*Atp1a3* $^{D801N/+}$ mice was consistently left-shifted, the θ frequency peak in B6C3.*Atp1a3* $^{E815K/+}$ mice gradually declined with age to the frequency observed in B6C3.*Atp1a3* $^{D801N/+}$ mice (Fig. 3F and G). Moreover, the θ power gradually increased in B6C3.*Atp1a3* $^{D801N/+}$ while it decreased in B6C3.*Atp1a3* $^{E815K/+}$ mice (Fig. 3H). In addition, we observed significant decreases in α and β power in both B6C3 AHC mice, but these did not overtly change with age (Fig. 3I and J). During periods of quiet wakefulness (lacking prominent θ activity, V1 cortical LFP example in Fig. S4C), however, only B6C3.*Atp1a3* $^{E815K/+}$ mice exhibited a gradual reduction in power across the θ, α and β frequencies (Fig. S4D, E, F and G).

Our EEG recordings show altered brain activity, with a reduction in the θ frequency peak in both B6C3 AHC mice, potentially reflecting an impairment in inhibitory neurotransmission. However, the distinct spectral power changes observed for the θ band for the two lines of B6C3 AHC mice suggest differences in synaptic strength with an increase in B6C3.*Atp1a3* $^{D801N/+}$ (increased θ power) and a decrease in B6C3.*Atp1a3* $^{E815K/+}$ (reduced θ power) mice. The observation of AHC variant specific brain activity changes may hint at potentially different mechanisms contributing to the development of distinct behavioral changes observed in B6C3 AHC mice. Importantly, B6C3.*Atp1a3* $^{E815K/+}$ mice revealed strikingly prominent electrophysiological changes (e.g., increased number of hippocampal spikes, occurrence of hippocampal-cortical giant spikes, SD events) that have previously been associated with an increased risk of epilepsy development (Buzsáki, 2015; Loonen et al., 2019; Motelow and Blumenfeld, 2009; Tamim et al., 2021; Zhen et al., 2021) and thereby, align with the increased seizure susceptibility observed in AHC patients. The observed epileptiform features and SD events in B6C3 AHC mice were not associated with profound behavioral seizure activity, nor can they explain the higher mortality of B6C3.*Atp1a3* $^{D801N/+}$ mice. However, our brain activity recordings were only performed over 3 days per time point in each mouse and none of the mice that died during the experiment (1 out of 7 D801N mice, 3 out of 11 E815K mice) happened to be in an EEG/video recording cage at the time of death. Neurophysiological abnormalities linked to mortality may require continuous and long-term EEG recordings to capture possible alterations that occur just prior to the unexpected death of B6C3 AHC mice.

2.4. Neurological changes in AHC mice affect neuronal health and neuroinflammation

To investigate whether the neurological defects in B6C3 AHC mice are accompanied by molecular and cellular alterations, we next performed transcriptome analysis on different brain regions including the cortex, hippocampus, brainstem and cerebellum of wild type, B6C3.*Atp1a3* $^{D801N/+}$ and B6C3.*Atp1a3* $^{E815K/+}$ mice (Fig. 4A). Aiming to detect potential molecular changes that are evoked upon neurological deficits, we analyzed adult B6C3 AHC mice (10 weeks) by which age mice are already susceptible to stress-induced paroxysmal spells, and exhibit motor defects and neurophysiological alterations, but prior to the overt onset of spontaneous deaths.

Relative to wild type mice, differential gene expression (DE) analysis revealed several significant (adj. $p \leq 0.05$) gene expression changes in B6C3 AHC mice, and we confirmed the RNA sequencing data for a subset of genes by quantitative RT-PCR (TaqMan) (Supplementary file 5, Fig. S5A and B). Similar to the ATP1A3 protein expression (Fig. S1F and G), no significant changes in *Atp1a3* gene expression were observed in B6C3 AHC mice (Supplementary file 5). To get a broader perspective of the gene expression changes, we visualized the intersection of the differentially expressed genes between AHC linked mutations and brain

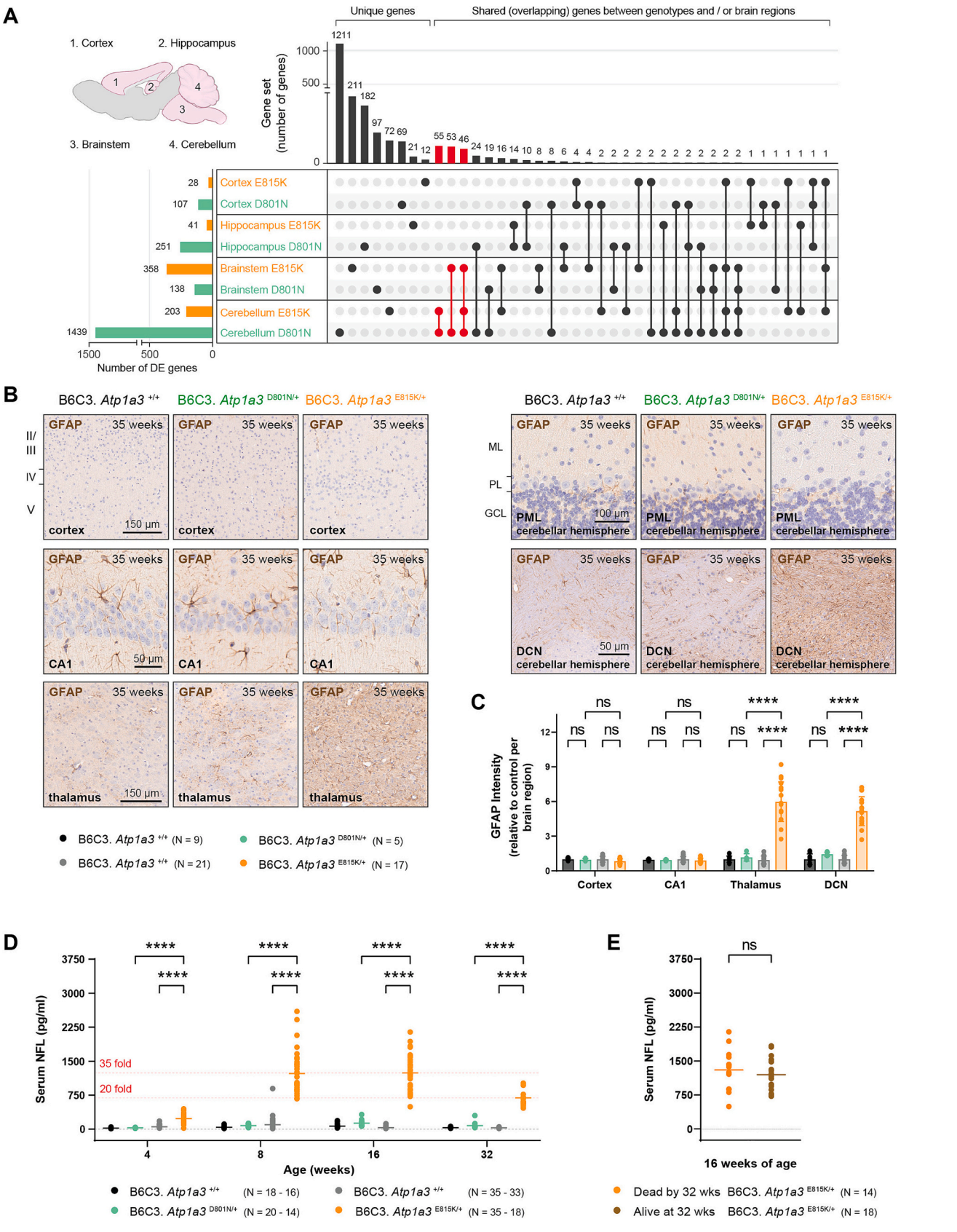

(caption on next page)

Fig. 4. Gene expression analysis of different brain regions in B6C3 AHC mice. (A) UpSet plot of differentially expressed (DE) genes (adj. $p \leq 0.05$) comparing AHC mutations and brain regions in mice. The anatomical locations of the analyzed mouse brain regions are shown in the upper, left corner. The total number of differentially expressed (adj. $p \leq 0.05$) genes for each brain region of B6C3.*Atp1a3* $^{D801N/+}$ (D801N, green) and B6C3.*Atp1a3* $^{E815K/+}$ (E815K, orange) mice are shown in the lower left corner. The number of unique genes and the intersection of genes are shown on the right-hand side. Notable gene intersections between genotypes and brain region are highlighted in red. (B) Immunohistochemistry using antibodies to glial fibrillary acidic protein (GFAP, astrocytes, brown) on parasagittal brain sections from 35-week-old wild type, B6C3.*Atp1a3* $^{D801N/+}$ and B6C3.*Atp1a3* $^{E815K/+}$ mice. Sections were counterstained with hematoxylin and higher magnifications of individual brain regions are shown. (C) Relative intensity of GFAP of wild type, B6C3.*Atp1a3* $^{D801N/+}$ and B6C3.*Atp1a3* $^{E815K/+}$ mice. Levels are relative to that of controls (wild type) from each cross and brain region. The data represent the mean ± SD. Wild type littermate controls for each mutant strain are shown (black and grey). (D) Longitudinal serum analysis of neurofilament light chain (NFL) of B6C3 AHC mice. The horizontal line for each group represents the mean. Wild type littermate controls for each mutant strain are shown (black and grey). (E) Comparison of serum NFL levels between B6C3.*Atp1a3* $^{E815K/+}$ mice that were either deceased at a later age (orange) or remained alive (brown). The horizontal line for each group represents the mean. Scale bars: 150 μm (cortex), 50 μm (CA1), 150 μm (thalamus), 100 μm (cerebellar hemisphere, PML) and 50 μm (cerebellar hemisphere, DCN). DE, differential gene expression; CA1, hippocampal cornu ammonis area 1; ML, molecular cell layer; PL, Purkinje cell layer; GCL, granule cell layer; PML, paramedian lobe; and DCN, deep cerebellar nuclei. Two-way ANOVA was corrected for multiple comparisons using Tukey method (C, D); Student's *t*-test (E). ns, not significant; **** $p \leq 0.0001$. The depicted mouse brain with specific brain regions was created with BioRender.com (A). See also Figs. S5, S6 and S7. (For interpretation of the references to colour in this figure legend, the reader is referred to the web version of this article.)

regions using an 'Upset plot'. Except for the brainstem, B6C3.*Atp1a3* $^{D801N/+}$ mice generally showed a higher number of differentially expressed genes than B6C3.*Atp1a3* $^{E815K/+}$ mice (Fig. 4A). When comparing the differentially expressed genes between D801N and E815K for each brain region, no significant gene overlap (hypergeometric density, Benjamini-Hochberg) was observed in the cortex, hippocampus, and brainstem, which parallels the Upset plot that revealed only a few shared genes between B6C3.*Atp1a3* $^{D801N/+}$ and B6C3.*Atp1a3* $^{E815K/+}$ mice (Fig. 4A). However, a significant ($p = 3.6558 \times 10^{-3}$, hypergeometric density, Benjamini-Hochberg) gene overlap was detected when comparing the cerebellar genes of B6C3.*Atp1a3* $^{D801N/+}$ (7.5 % of D801N genes overlap with E815K) and B6C3.*Atp1a3* $^{E815K/+}$ mice (53 % of E815K genes overlap with D801N) (Fig. 4A). Although not significant ($p = 0.06313$), a moderate gene overlap was also observed between genes of the cerebellum and brainstem in B6C3.*Atp1a3* $^{E815K/+}$ mice (Fig. 4A), highlighting that while most of the gene expression appeared to be unique in B6C3 AHC mice, at least a subset of the differentially expressed genes are affected in multiple brain regions by either mutation (red, Fig. 4A).

To identify pathways that might be linked to the gene expression changes, we performed KEGG and IPA pathway analysis on the differentially expressed (adj. $p \leq 0.05$) genes of B6C3.*Atp1a3* $^{D801N/+}$ and B6C3.*Atp1a3* $^{E815K/+}$ mice. Strikingly, immune response and inflammation related pathways were highly enriched and represented most of the top pathways in the cerebellum of B6C3.*Atp1a3* $^{E815K/+}$ mice (pathways are highlighted in red, Fig. S5C and D). However, immune system related pathways showed a noticeable lower enrichment in the cerebellum of B6C3.*Atp1a3* $^{D801N/+}$ mice and mirrored the pathway enrichment in the brainstem of B6C3 AHC mice (Fig. S5C, D, E and F).

The comparison with neuroinflammatory genes that were previously identified in CNS tissues of mouse models with various neurological and neurodegenerative conditions (Supplementary file 7) (Chiu et al., 2013; Holtman et al., 2015; Ishimura et al., 2016; Orre et al., 2014) revealed that approximately 18 % and 27 % of the differentially expressed cerebellar genes (adj. $p \leq 0.05$) were neuroinflammation genes in B6C3.*Atp1a3* $^{D801N/+}$ and B6C3.*Atp1a3* $^{E815K/+}$ mice, respectively (Fig. S6A and B). Interestingly, expression of these neuroinflammatory genes was significantly increased (fold change) in both B6C3 AHC models (Fig. S6C). Nevertheless, B6C3.*Atp1a3* $^{E815K/+}$ showed a higher upregulation (fold change) of neuroinflammatory genes compared to B6C3.*Atp1a3* $^{D801N/+}$ mice (Fig. S6C). Moreover, only 7 % of the inflammation genes showed an increase in gene expression greater than 2-fold in B6C3.*Atp1a3* $^{D801N/+}$ while 35 % of neuroinflammatory genes showed an upregulation greater than 2-fold in B6C3.*Atp1a3* $^{E815K/+}$ mice. In addition, expression of neuroinflammatory genes was also significantly increased in the brainstem of B6C3.*Atp1a3* $^{E815K/+}$ mice (Fig. S6D). Thus, similar to the pathway enrichment observations (Fig. S5C, D, E and F), the magnitude and/or activation of neuroinflammatory related gene expression changes may differ between B6C3 AHC mice and brain regions. Because the previously identified neuroinflammatory genes included those of microglia and astrocyte origin (Supplementary file 7), these data suggest that mutations in the neuron specific ATP1A3 may also elicit cellular responses in cell types beyond ATP1A3 expressing neurons.

Since the transcriptome analysis revealed inflammation related gene expression changes, we performed immunostaining using antibodies against common neuroinflammation markers including GFAP (glial fibrillary acidic protein, astrocytes) and Iba1 (ionized calcium-binding adapter molecule 1, microglia) (Amalia, 2021; Cao et al., 2021; Ishimura et al., 2016; Wang et al., 2023; Young et al., 2013). We did not observe overt changes in GFAP or Iba1 in the cortex and hippocampus of B6C3 AHC mice (Fig. 4B and C, Fig. S7A and B), which aligns with the lack of enrichment of immune related pathways in those brain regions. However, GFAP and Iba1 staining were strongly increased in the thalamus and deep cerebellar nuclei (DCN) in the cerebellum of B6C3.*Atp1a3* $^{E815K/+}$ mice (Fig. 4B and C, Fig. S7A and B). Moreover, B6C3.*Atp1a3* $^{D801N/+}$ mice only showed a significant increase in Iba1 reactivity in the deep cerebellar nuclei of the cerebellum whereas Iba1 and GFAP levels in the other regions of the brain remained similar to wild type mice (Fig. 4B and C, Fig. S7A and B). Interestingly, reactivity of these neuroinflammation markers was significantly stronger in B6C3.*Atp1a3* $^{E815K/+}$ compared to B6C3.*Atp1a3* $^{D801N/+}$ mice (Fig. 4C, Fig. S7B) and paralleled the directionality of the transcriptomic inflammatory pathways observed in B6C3 AHC mice (Fig. S5C and D, Fig. S6A, B, C, and D).

Furthermore, we longitudinally measured serum levels of neurofilament light chain (NFL) as a means to monitor 'brain and neuronal health' in B6C3 AHC mice. NFL is a neuron specific cytoskeletal protein, which has gained great attention as an unspecific biomarker to assess disease progression and pathology, as well as treatment response in animal models and humans. Increased NFL levels (e.g., in the cerebrospinal fluid, serum and plasma) have been observed upon neuronal and axonal damage, brain lesions, astrogliosis and immune cell extravasation (neuroinflammation), and impairment of the blood-brain-barrier integrity (Barro et al., 2020; Bavato et al., 2024; Freedman et al., 2024; Jing et al., 2024; Uher et al., 2021; Van Den Bosch et al., 2022; Yuan and Nixon, 2021). In B6C3.*Atp1a3* $^{D801N/+}$ mice, serum NFL levels remained comparably low compared to those observed in wild type mice and only showed a statistically significant (p-value = 0.0218) increase of ~1.85 fold at 16 weeks of age (Fig. 4D). In contrast, serum NFL levels progressively increased and leveled to a ~ 20-fold increase in B6C3.*Atp1a3* $^{E815K/+}$ mice (Fig. 4D). In the case of certain other neurological disorders, increased NFL levels negatively correlated with survival while in others, the levels coincided with specific pathological cellular or functional alterations of the brain (Bacioglu et al., 2016; Bavato et al., 2024; Gravesteijn et al., 2019; Jung and Damoiseaux, 2023; Kirschen et al., 2020; Nguyen et al., 2022). In B6C3 AHC mice, serum levels of NFL did not predict or correlate with the observed survival defects

(Fig. 4D and E, Fig. 1A and B). Regardless, the increase in NFL levels coincides with functional (e.g., motor and neurophysiological function) and histological (e.g., neuroinflammation) differences that are more severe in B6C3.*Atp1a3* $^{E815K/+}$ compared to B6C3.*Atp1a3* $^{D801N/+}$ mice. Thus, changes in NFL levels may not holistically capture disease severity in B6C3 AHC mice that is reflected or assumed by their mortality, but perhaps, points to the differential severity of specific functional and/or morphological changes in the brain, which are linked to certain AHC variants.

3. Discussion

AHC patients with the p.D801N or p.E815K variant exhibit paroxysmal spells by the age of 18 months. When comparing the two AHC variants, p.E815K patients present an earlier onset, a further delay in unsupported sitting and walking, and more severe cognitive impairment, dystonia and seizures (Capuano et al., 2020; Ford et al., 2023; Panagiotakaki et al., 2015; Viollet et al., 2015). In addition, patients with the p.E815K variant have a significantly higher occurrence (~3 times) of status epilepticus (prolonged or repetitive seizures), suggesting that a higher pathogenicity may be linked to the p.E815K variant relative to other AHC variants (Capuano et al., 2020; Ford et al., 2023; Panagiotakaki et al., 2015; Viollet et al., 2015). A similar notion of p.E815K causing more severe neurological abnormalities was suggested for the previously developed B6J AHC mice (D801N and E815K) with the B6J E815K mice revealing rotarod defects and increased freezing behavior compared to B6J D801N mice (Helseth et al., 2018; Hunanyan et al., 2014). However, comparing and defining similarities or dissimilarities of AHC linked mutations in B6J AHC mice remains difficult, at least in part, because of challenges that arose from the severe mortality and/or differences in experimental testing paradigms.

B6C3.*Atp1a3* $^{E815K/+}$ mice showed overt electrophysiological abnormalities (e.g. spikes and spontaneous SDs) compared to B6C3.*Atp1a3* $^{D801N/+}$ mice, fitting with the higher susceptibility to epilepsy observed in p.E815K patients. Notably, B6C3 wild type mice exhibited a higher incidence of SWDs compared to B6C3 AHC mice. The incidence and a wider variation of SWDs in B6C3 mice is consistent with the mice being a hybrid between C3H/HeJ and C57BL/6J mice and highlights the complex interaction of genetic factors between C3H/HeJ and C57BL/6J that contribute to the presence of SWDs (Frankel et al., 2005). However, why B6C3 AHC mice show fewer SWDs compared to B6C3 wild type mice remains unclear.

In addition, motor (e.g., rotarod performance) and molecular defects (e.g., NFL, neuroinflammation) were also more affected in B6C3.*Atp1a3* $^{E815K/+}$ mice. While these deficits align with the severe impact of the p.E815K variant, spontaneous lethality and hypothermia induced paroxysmal episodes were instead more prominent in B6C3.*Atp1a3* $^{D801N/+}$ mice. Furthermore, differential responses were also observed in the open field testing (e.g., horizontal and vertical activity) and during electrophysiology recordings (e.g., θ power) of B6C3 AHC mice. These data imply that tractable and distinct alterations for specific AHC variants can be detected in mice and perhaps, phenotypic severity may not merely be a function of a specific genotype (e.g., p.E815K being the most severe variant) but may also depend on the specific phenotypic defect that is investigated. Recently, the third most common AHC variant (p.G947R) was introduced in B6J mice and it also caused electrophysiological defects and stress induced dystonia (Hawkins et al., 2024). Interestingly, B6N D801Y mice, which carry an ATP1A3 variant linked to RDP/AHC, and B6J G947R mice showed an increase in rotarod performance that is in contrast to the reduced rotarod performance observed in B6C3 D801N and E815K mice here (Hawkins et al., 2024; Liu et al., 2024). Although these strains differ in their genetic background, which to a certain extent could limit a fair comparison, these data may still hint to specific changes that are mediated in an AHC variant dependent manner. Thus, continuing efforts to interrogate and systemically compare alterations of mice that harbor different pathogenic AHC variants may provide viable approaches to identify and delineate faulty neuronal circuits regulating dystonia, seizure and/or motor activity defects in AHC (summary of phenotypic defects in D801N and E815K mice, Supplementary file 9).

Even though ATP1A3 expression is restricted to neurons in the brain (Dobretsov et al., 2019; Gokce et al., 2016; Jiao et al., 2022; Smith et al., 2021), adding to the investigation of neuronal function is perhaps the interaction with non-neuronal cells of the brain. The analysis of brains of B6C3 AHC mice revealed expression and activation of inflammatory markers in different brain regions. Whether these neuro-inflammatory changes have functional implications is unclear and will require further investigation. In the case of other neurological disorders, neuroinflammation can be protective or deleterious when chronic and uncontrolled (Adamu et al., 2024; DiSabato et al., 2016). Numerous studies have highlighted the complex interaction between epilepsy and inflammation, in which neuroinflammation can be cause or consequence of seizures/epilepsy (Eyo et al., 2017; Foiadelli et al., 2023; Pracucci et al., 2021; Sanz et al., 2024; Suleymanova, 2021). Astrocytic and microglial ion pumps and channels can act as buffer systems of excessive extracellular ions during seizures and provide anti-seizure properties (Du et al., 2018; Eyo et al., 2014; Zhao et al., 2022). Nevertheless, cytokines that are released by astrocytes and microglia also have excitatory effects and may further burden brain excitability and/or cause neuronal excitotoxicity (Foiadelli et al., 2023; Liu et al., 2020; Sanz et al., 2024; Villasana-Salazar and Vezzani, 2023). Thus, anti-inflammatory drugs are also considered as potential treatment options when anti-convulsant drugs fail to show disease altering outcomes or patients have drug-resistant seizures/epilepsy (Pracucci et al., 2021; Radu et al., 2017; Sanz et al., 2024).

Deterioration in motor and intellectual function has been observed in some AHC patients and sometimes coincides with cerebral and cerebellar atrophy (Neville and Ninan, 2007; Paciorkowski et al., 2015; Sabouraud et al., 2019; Saito et al., 2010; Sasaki et al., 2014; Sweney et al., 2015). Irreversible atrophy is particularly more often noticed in p.E815K patients with status epilepticus (Grillo, 2015; Li et al., 2015; Sasaki et al., 2017; Sasaki et al., 2014). Because of the symptomatic heterogeneity and because progressive decline in neurological function is not always observed in AHC patients (Panagiotakaki et al., 2010; Pavone et al., 2022a), it is still unclear whether pathogenic AHC variants cause progressive defects as part of the primary Na^+/K^+-ATPase defect, or perhaps, such defects are related to repeated paroxysmal episodes.

Interestingly, B6C3.*Atp1a3* $^{E815K/+}$ mice exhibited progressive deficits in motor function (e.g., rotarod performance), neurophysiology (e.g., SD, hippocampal spikes and giant spikes) and serum NFL levels in contrast to B6C3.*Atp1a3* $^{D801N/+}$ mice. Importantly, measurements for our studies were obtained from naïve and separate cohorts of mice with the aim to measure baseline phenotypic defects and minimize excessive stress that could affect functional readouts since B6J AHC mice were highly susceptible to stress (e.g., routine and experimental handling). While progressive defects can already be observed under baseline conditions, interrogating the neurological function of B6C3 AHC mice when intentionally also introducing stress paradigms (e.g., hypothermia-induced paroxysmal episodes, HIP) may provide opportunities to systematically test for the contribution of severe and repetitive paroxysmal episodes in AHC.

How different mutations in *ATP1A3* can lead to different phenotypic deficits and/or cellular responses is unclear. The D801N and E815K mutations abolish the catalytic activity of the mutant ATP1A3 protein *in vitro*. Interestingly, the pathogenic p.D801Y variant observed in RDP and mild AHC patients reduces ATP1A3 (α3) protein expression by ~20 % and α3-specific activity by ~75 % in the brain of B6N D801Y mice (Holm et al., 2016; Liu et al., 2024), which is less drastic compared to the impairment of α3 activity observed in B6C3 D801N mice and aligns with previous *in vitro* investigations (De Carvalho Aguiar et al., 2004; Heinzen et al., 2012). However, the mere functional impairment of ATP1A3 (loss of catalytic activity) does not correlate with the disease severity

observed in ATP1A3 patients (Arystarkhova et al., 2019; Lazarov et al., 2020). While both p.D801N and p.E815K ATP1A3 are catalytically inactive, previous studies found that the p.D801N variant can still bind ouabain while the p.E815K variant results in a severely affected loss-of-function protein, which may contribute, in part, to the severity observed in patients (Heinzen et al., 2012; Weigand et al., 2014). Nevertheless, the dominant nature of AHC variants suggest that additional mechanisms may contribute to disease pathology and may include changes in protein folding, biosynthesis, and ATP1A3 membrane trafficking (Arystarkhova et al., 2021; Arystarkhova et al., 2019). Interestingly, recent studies suggested that human ATP1A3 interacts with RNA-binding proteins and proteins regulating translation, suggesting that ATP1A3 may potentially also play a role in RNA translation (Fujii et al., 2024). Whether pathogenic AHC variants alter such protein interactions and/or may even evoke aberrant interactions of the mutant protein, which has been observed for other genetic disorders such as Charcot-Marie-Tooth (CMT) disease, is unknown (Bervoets et al., 2019; Kalotay et al., 2023; Sun et al., 2021). However, these data and the increasing identification of non-canonical (non-catalytic) functions observed for other proteins may open the path for investigations beyond the 'canonical' ion pump activity of ATP1A3 (Fujii et al., 2024; Huangyang and Simon, 2018; Jeffery, 2020; Pan et al., 2021; Snaebjornsson and Schulze, 2018).

Lastly, B6C3 AHC mice also provide alternative mouse models for translational and pre-clinical AHC research, and the mouse models have been donated to public mouse repositories (JAX/MMRRC). Notably, the introduction of hybrid vigor reduced early mortality and lethal episodes that occur during animal handling while the B6C3 D801N and B6C3 E815K mouse models still develop clinically relevant phenotypes including spontaneous death, hypothermia induced paroxysmal episodes (HIP), and motor, neurophysiological, and histological defects. A similar beneficial effect of hybrid vigor on animal fitness has also been recently observed for the AHC G947R mice (Hawkins et al., 2024). In the context of pre-clinical animal testing, behavior (e.g., rotarod and open field) and histological testing of mice present standardized, feasible and/or high throughput measurements. In comparison, HIP testing is generally more time consuming, particularly when considering large scale efficacy studies. However, these experiments are compatible with camera systems to record the animal behavior during HIP recovery and in turn, simplify or at least add resolution when assessing the therapeutic response in mice. Moreover, biomarker discovery and development have become increasingly critical for both pre-clinical and early phase clinical trials to assess safety, efficacy or to molecularly demonstrate therapeutic engagement. The ability to longitudinally monitor disease and experimentally manipulate deficits in animal models enables future biomarker exploration when screening of candidates in patient populations is challenging due to the limited number of patients, genetic, environmental or symptomatic heterogeneity. Although other ATP1A3 mouse models have been previously generated, expanding the existing repertoire (summarized by Ng et al., 2021) with the inclusion of these novel AHC models may not only assist in overcoming earlier experimental limitations but may also put forward new platforms for basic and translational ATP1A3 research.

4. Materials and methods

4.1. Mouse strains and lines

Several mouse strains and lines have been generated as part of this study and the strain details are outlined below. For the generation of B6J-*Atp1a3* $^{D801N/+}$ mice (C57BL/6J-*Atp1a3*^{em3Lutzy}/Lutzy or *Atp1a3* $^{D801N,\ L802L}$), plasmids encoding a signal guide RNA to introduce the D801N point mutation in exon 17 of the *Atp1a3* gene and the Cas9 nuclease were introduced into the cytoplasm C57BL/6J-derived fertilized eggs (B6J, JR #664, The Jackson Laboratory). An additional silent nucleotide change (CTG to CTA, L802L) was introduced as part of the CRISPR/Cas9 inactivating strategy. Targeted heterozygous embryos were transferred to pseudo-pregnant females. Pups were analyzed for correct targeting and the absence of off targets by sequencing and PCR for further breeding. Survival data for this strain were previously provided to support other ATP1A3 research studies (Liu et al., 2024). The congenic B6.129(Cg)-*Atp1a3*$^{tm1.1Mika}$/Mmjax (also known as 'Matb' or E815K *knock in* mice) were previously generated and have been kindly provided by Dr. Mohamad A. Mikati (Helseth et al., 2018) (MMRRC #069591 at The Jackson Laboratory, MGI:6856863).

Because the B6J AHC mice were highly susceptible to early, sudden and/or unexpected death, and hindered the maintenance of either strain, we transferred the corresponding AHC mutations onto a hybrid vigor genetic background using *in vitro* fertilization (IVF). For the generation of B6C3.*Atp1a3* $^{D801N/+}$ mice (B6C3-*Atp1a3*^{em3Lutzy}/Mmjax), an IVF expansion utilizing sperm from heterozygous C57BL/6J-*Atp1a3*^{em3Lutzy}/Lutzy males and C3H/HeJ (C3H, JR #659, The Jackson Laboratory, MGI:2159741) females as oocyte donors was performed and produced wild type (B6C3.*Atp1a3* $^{+/+}$) and heterozygous mutant (B6C3.*Atp1a3* $^{D801N/+}$) mice ([B6xC3H]F1). To ensure sufficient heterozygosity between the B6J and C3H genetic backgrounds for the subsequent strain maintenance, heterozygous B6C3.*Atp1a3* $^{D801N/+}$ males (carrier) are crossed to B6C3F1/J (JR #100010, The Jackson Laboratory, MGI:5654213) females every generation and the resulting progeny are subject to experimental testing ([carrier x B6C3F1/J]NX with N referring to constant backcross with B6C3F1/J mice and X referring to the number of generations). Sperm ([carrier x B6C3F1/J]N1p) has been cryopreserved (p) and donated to the MMRRC at the Jackson Laboratory and is publicly available (MMRRC #071287 at The Jackson Laboratory, MGI:7461667, or JAX JR# 38294). It is important to note that the B6C3.*Atp1a3* $^{+/+}$ and B6C3.*Atp1a3* $^{D801N/+}$ mice are a hybrid between the B6J and C3H inbred strains and therefore carry genetic polymorphisms derived from either inbred strain.

For the generation of B6C3.*Atp1a3* $^{E815K/+}$ mice (*Atp1a3*$^{tm1.1Mika}$/LutzyMmjax), an IVF expansion utilizing sperm from heterozygous B6.129(Cg)-*Atp1a3*$^{tm1.1Mika}$/Mmjax (MMRRC #069591 at The Jackson Laboratory, MGI:6856863) males and C3H/HeJ (C3H, JR #659, The Jackson Laboratory, MGI:2159741) females as oocyte donors was performed and produced wild type (B6C3.*Atp1a3* $^{+/+}$) and heterozygous mutant (B6C3.*Atp1a3* $^{E815K/+}$) mice ([B6xC3H]F1). To ensure sufficient heterozygosity between the B6J and C3H genetic backgrounds for the subsequent strain maintenance, heterozygous B6C3.*Atp1a3* $^{E815K/+}$ males (carrier) are crossed to B6C3F1/J (JR #100010, The Jackson Laboratory, MGI:5654213) females every generation and the resulting progeny are subject to experimental testing ([carrier x B6C3F1/J]NX with X referring to the generation). Sperm ([B6 x C3H]F1p) has been cryopreserved (p) and donated to the MMRRC at the Jackson Laboratory and is publicly available (MMRRC #071376 at The Jackson Laboratory, or JAX JR #38457). It is important to note that the B6C3.*Atp1a3* $^{+/+}$ and B6C3.*Atp1a3* $^{E815K/+}$ mice are a hybrid between the B6J and C3H inbred strains and therefore carry genetic polymorphisms derived from either inbred strain.

Upon discovery of the reduction in fragility of B6C3 AHC mice and to support potential applications for other ATP1A3 researchers, we publicly shared this information and the data with the ATP1A3 and AHC community through the annual ATP1A3 symposium in 2022 and 2023, and the public mouse strain catalog of the Jackson Laboratory.

Mice were genotyped at birth, wean age (~postnatal P28), and triple confirmed when they reached the expected study end point (e.g., necropsy for tissues collection and/or histology). The genotyping primers and PCR conditions are listed below for each mutant allele and are applicable regardless of the genetic background. The Jackson Laboratory Animal Care and Use Committee, the ethical committee of the Leiden University in accordance with ARRIVE guidelines and EU Directive approved all mouse protocols.

A) D801N mutation.

Common Forward: 5' CTC TTG GCA CCA TCA CCA TC'3.

Common Reverse: 5′ TTT AGT AGC AGC CAG GCT TAC C′3.
WT Probe (HEX): 5’ CTG CAT TGA CCT GGG TAC C′3.
D801N mutant Probe (FAM): 5’ TCT GCA TTA ACC TAG GTA CCG AC’3.
B) E815K mutation.
Common Forward: 5’ ACT CAC ACA GCC TGC CTC TC’3.
Common Reverse: 5’ CCT CTT CAT GAT GTC GCT CTC’3.
WT Probe (HEX): 5′ TGG CCT ACG AGG CTG C′3.
E815K mutant Probe (FAM): 5′ TGG CCT ACA AGG CTG CC’3.

Reaction				Cycling		
Step	**Reaction Component**			**Step**	**Temp.**	**Time**
1	1x Kapa Probe Fast QPCR			1	95	3 min
2	ddH2O			2	95	5 sec
3	Forward Primer 0.4 uM			3	60	15 sec
4	Reverse Primer 0.4 uM			4	repeat 2-3 for 40 cycles	
5	WT Probe 0.15 uM			5	40	hold
6	Mutant Probe 0.15 uM					
7	DNA					

4.2. Mouse cohorts

Several cohorts of mice were generated as part of this study and the details are outlined below. Our hybrid mouse lines are maintained through the cross with B6C3F1 mice in every generation to ensure sufficient heterozygosity between the B6J and C3H strains, to prevent homozygosity from getting fixed, and to segregate within our mouse lines. Even though a given locus (strain specific polymorphism e.g., C3H specific Pde6b-rd1 variant) has the chance of homozygosity with a lower frequency, we still considered various factors for the choice of our behavioral tests. Considerations included that both B6J and C3H strains are known to perform the behavioral test of choice. In the context of e.g., the Pde6b-rd1 variant (visual impairment), C3H mice with and without retina degeneration can perform the open field and rotarod test with equivalent performance (Voller et al., 2014). The consideration of the Pde6b-rd1 variant did not apply for survival, HIP, grip, ECG, and electrophysiology testing. Mice across multiple generations ([carrier x B6C3F1/J]N1–7) were subjected to testing. All testing was done during daylight hours and performed using mice of either sex.

1. *Body weight cohort*. Body weights shown were recorded weekly starting from birth up to ~32 weeks of age. Mice were not subjected to any other behavioral testing.
2. *HIP cohort*. HIP experiments shown were performed on mice at 6 and 12 weeks of age. Mice were not subjected to any other behavioral testing.
3. *Rotarod cohort*. Rotarod experiments shown were longitudinally performed on mice at 10 and 12 weeks of age. Mice were not subjected to any other behavioral testing.
4. *Open field cohort*. Open field experiments shown were performed on mice at 15 weeks of age. Mice were not subjected to any other behavioral testing.
5. *Blood collection, grip strength, rotarod and necropsy cohort*. Retro-orbital blood collection (for NFL analysis) was performed on mice at various ages, grip testing at 16 weeks of age, rotarod testing at 24 weeks of age, and then, were collected for necropsy at 35 weeks of age. Mice were not subjected to any other behavioral testing.
6. *ECG cohort*. Mice were tested at 22 weeks of age for ECG testing.
7. *Electrophysiology cohorts*. Mice were longitudinally subjected to electrophysiological testing (e.g. epileptiform activities, PSD analysis and spontaneous SD) at 6, 10 and 14 weeks of age. Mice were not subjected to any other behavioral testing.
8. *Molecular biology cohorts*. Tissue samples from mice were collected for molecular analysis. Mice were not subjected to any other behavioral testing.
9. *DIVA cohorts*. Mice were longitudinally monitored between 13 and 22 weeks of age. Mice were not subjected to any other behavioral testing.
10. *Survival*. The survival of all generated and sampled mice (birth to pre-defined study end) was monitored. The survival of B6C3 AHC mice has not been monitored and/or tested past 8.5 months of age. The survival data does not include data of breeders because the recording of litters of the breeder colony only occurred between P10-P23, only male mice were sampled and genotyped, and male breeders were replaced at ~14–16 weeks of age to refresh breeding units. The survival of mice subjected to electrophysiology studies is not included because some, but not all mice, were internationally shipped, and because test subjects required brain surgery for the probe implantation.

4.3. Survival testing

In addition to the routine welfare check, animals were monitored (2–3 times per week) from birth on. For spontaneous deaths, mice were found dead without any prior indication of welfare and/or health concerns. In addition, mice were monitored for their overall health by assessing the body condition score (BCS) (Foltz and Ullman-Cullere, 1999). In the presence of a lowering BCS, mice were provided with a diet gel (Nutra-Gel, Bio-Serv) to support health and the overall body condition, particularly in the case of B6C3.*Atp1a3* $^{E815K/+}$ mice. Nevertheless, mice that reached BCS ≤ 2, the defined humane end point, were recorded as ‘death’ and included in the survival curve. Although spontaneous and unexpected deaths were observed in B6C3.*Atp1a3* $^{E815K/+}$ mice, they required humane euthanasia as the study end point (‘death’) due to low BCS. Thus, survival data include spontaneous death and death due to low BCS.

4.4. Continues video monitoring of animal activity (DIVA cage system)

The Digital In Vivo Alliance (DIVA) represents a consortium that brings together AbbVie, BioMarin, Calico Life Sciences, Novartis, and The Jackson Laboratory as the founding members. By utilizing continuous video recordings of mice in their home cage together with the application of AI and machine learning, the DIVA consortiums aid to provide a dynamic and holistic approach for the development, identification and monitoring of digital biomarkers (animal movement and activity) of mice for pre-clinical in vivo research. Although the development of algorithms, and the application and validation of digital biomarkers are on-going efforts (see the link to the white paper), in the meantime, we utilized these cages with their built-in camera system (bird's eye view, see examples Supplementary file 1 and Supplementary file 2) to continuously monitor and record the behavior of our mice in their home cage. Animals housed in DIVA cages are maintained under equivalent conditions compared to animals that are housed in cages that lack a built-in camera. In contrast to other cage systems with food and water access from the top, food and water reservoirs are located to the side (wall of cage, see diagram below) of the DIVA cages.

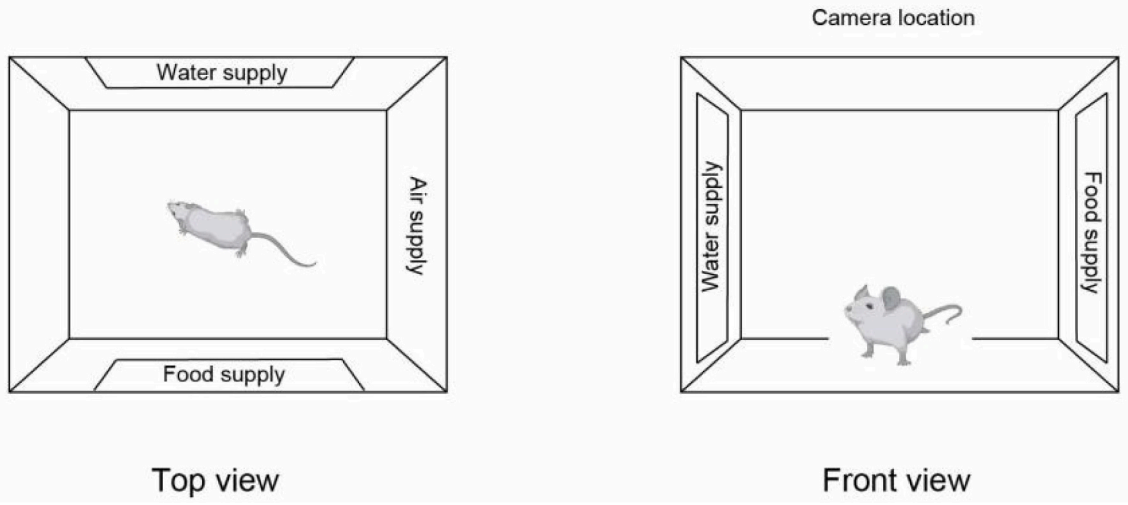

Link to White Paper: https://resources.jax.org/white-papers/analytical-validation-of-digital-in-vivo-mouse-detection-identification-and-movement-in-the-envision-platform

4.5. Hypothermia induced paroxysmal episodes (HIP)

We adopted the previously described hypothermia paradigm with some modifications (Isaksen et al., 2017; Pizoli et al., 2002). A clear plastic box (30 × 30 × 14 cm with a floor area of 728 cm^2) was filled with 5 °C ± 0.2 °C cold water (monitored via thermometer) up to a height of ~4 cm to ensure that the core of the mouse body is submerged in the water but the mouse retains the ability to touch the floor of the box with at least their hind limbs and therefore, avoid the risk of drowning. The body weight and rectal body temperature were measured. The 'duration in water' was determined based on body weight (see table below) to accomplish a comparable body temperature reduction of at least 10 °C. Note: The body weight difference between wild type and mutant mice becomes increasingly bigger with age and accommodating a comparable reduction in body temperature between genotypes would have required mice (e.g., wild type) to exceed the 'duration in water' past 5 min. Thus, HIP experiments were not performed on mice past 12 weeks of age to avoid potential welfare and health concerns.

Sex	Body weight	Duration in water
Females/Males	Less than 20 g	2 min
Females/Males	20 - 30 g	3 min
Females/Males	More than 30 g	5 min

While restrained, the mouse was transferred into the water and then slowly released (timer to start 'duration in water'). Subsequently, the mouse was taken out of the water bath, excess of water removed through a paper towel, the rectal body temperature was immediately measured (0 min), and the mouse was placed in the 'recovery station' for the observation of paroxysmal episodes. One side (floor area of 333 cm^2) of a duplex cage functioned as the 'recovery station' (one mouse per 'recovery station'). The 'recovery station' was on top of a heating pad, which was set to 37 °C. Half of the floor of the 'recovery station' was covered with cage bedding while the other half remained bare of bedding. The mouse was placed on the bare side to avoid the cage bedding causing a visual obstruction for the operator (video example, see Supplementary file 3). Upon recovery of mobility, mice generally moved into bedding (e.g. hiding, grooming, ….). The rectal body temperature was measured at 15-, 30- and 60-min post water exposure. The mouse was moved from the 'recovery station' back into the home cage upon complete recovery (body temperature, normal mobility and mouse

behavior). The scoring of paroxysmal episodes (dystonia- and convulsion-like events) was performed post water exposure (start of 'recovery period') and we adopted a scoring system (see table below) with some modifications based on previous studies (Pizoli et al., 2002).

Dystonia-like events			Convulsion-like events
HIP Score	**Pizoli et al, 2002**	**This study**	**This study**
0	No motor abnormalities and no dystonia	No motor abnormalities and no dystonia	Recorded as "Yes" or "No" independent of dystonia-like events (score)
1	Slowed motor behavior but no dystonia	Slowed motor behavior but no dystonia	
2	Limited movement/ambulation, dystonic posture/event when disturb	Dystonia only occurs when the mouse is "disturbed" such as handeling during body temperature measurement (distinction to mere "hypothermic" events)	
3	Moderate impairment of movement, frequent and spontaneous dystonic events/postures	Dystonia occurred, animals retain abillity to hold/balance/right themself, dystonic events may occur frequent/multiple times	
4	Severe impairment of movement, sustain and frequent dystonic events/postures	Dystonia occurred, animals occasionaly retain abillity to hold/balance/right itself, dystonic events are longer lasting and may occur frequent/multiple times	
5	Prolonged immobility in dystonic postures/events	Dystonia occurred, animals fail to retain abillity to hold/balance/right itself, e.g. lay flat on stomach, back or side, no signs to correct position, dystonic events are long lasting	

Note: Since Pizoli et al., 2002 included the option that defects may occur upon 'disturbance' (score 2), we wanted to allow for the possibility that hypothermia on its own is not sufficient to induce events but instead also requires further 'disturbance'. Therefore, we defined the score of 2 as dystonia-like events that occur upon 'disturbance'. Because operators are required to record the body temperature (physical handling) at consistent and pre-defined time intervals for any mouse, we utilized this as 'disturbance'. Thus, a score of 2 would only be recorded if events immediately followed the measurement of body temperature. However, we did not observe such events and therefore, our data lack observations for a score of 2 (Fig. 1D).

4.6. Rotarod

Mice were habituated to the testing room one hour prior to testing with the rotarod on and rotating (Ugo Basile Rotarod for Mouse). The apparatus was cleaned before and in between each mouse with 70 % ethanol. Mice were tested for four consecutive trials of accelerating rotarod starting at 5 RPM and ramping up to 40 RPM over 300 s. Latency to fall for each of the four trials was recorded with a 45 s rest period between each trial. Day one is considered training day, followed by the same protocol on the subsequent day which is considered testing day (Fig. 2A). The latency from the testing day trials 2, 3, and 4 were averaged and reported as latency to fall for each mouse. For the assessment of motor learning function (Fig. S2A), the exact same protocol was used with additional, consecutive test days (1 training day and 3 testing days).

4.7. Grip strength

A commercially available grip-strength meter (Bioseb) attached to a wire grid was used to measure front paw and hind paw peak grip strength (kg). Mice were weighed and allowed to acclimate to the testing room for a minimum of 60 min before testing. For fore paw testing, mice were held by their tails and lowered toward the grid to allow for the mouse to grip the grid with its forepaws. The animal was firmly pulled horizontally away from the grid. With hind paw testing, each mouse was restrained, and hind paws were dragged the length of the grid and peak grip strength was recorded. An average of 3 trials served as the final peak force. The grip strength is shown with and without normalization to the mouse body weight.

4.8. Open field

Open field arenas used in this study were squares (40 × 40 × 40 cm) and made from clear Plexiglass. LED lights indirectly illuminated the arenas at ranges of 100–500 ± 20 lx. The chambers were vented, and sound attenuated. Mice were habituated to the room for 60 min prior to the test. One mouse was placed in the center of each arena, and vertical and horizontal activity were recorded by beam breaks across two levels in infrared beams using the Fusion software (OmniTech Electronics). Mice were recorded for 60 min, and the arenas were cleaned with 70 % ethanol between subjects within a single testing day. Several readouts were obtained from the open field analysis, and the details are listed below.

1. *Total distance traveled.* The total distance that the subject has traveled.
2. *Total movement time.* The length of time that the subject spent in activity. Activity is defined as a period in which ambulation and/or stereotypy occurred.
3. *Total rest time.* The length of time that the subject spent at rest. A resting period is defined as a period of inactivity greater than or equal to 1 s.
4. *Stereotypic episode count.* The number of beam breaks due to stereotypic activity. If the animal breaks the same beam (or set of beams) repeatedly then the monitor considers that the animal is exhibiting stereotypy. This typically happens during grooming or head bobbing.
5. *Vertical episode count.* This is incremented by 1 each time the animal rears. The animal must go below the level of the vertical sensor for at least 1 s before the next rearing can be registered.
6. *Total margin time.* Time spent by the animal in proximity to the walls of the cage. This area is defined as the exterior 4 × 16 and 16 × 4

matrices for the left right bottom and top regions. The margin reflects 75 % of the open field arena.

7. *Total center time.* The total time spent in the center portion of the cage. This area is defined as the center 8 × 8 square matrix plus the coordinates between the outermost beams of the area and the adjacent non-area beams. The center reflects 25 % of the open field arena.

4.9. Electrocardiogram

ECG studies were performed as previously described (Oestereicher et al., 2023). Briefly, mice were anesthetized in the induction chamber with 2–3 % isoflurane. Once the mouse was in lateral recumbency and unable to right itself, eye lubricant was applied, and the animal was transferred to a nosecone for maintenance with 1–2 % isoflurane. Anesthetized mice were positioned supine on a warming pad apparatus that maintained the animal's core temperature at 37 °C. Surface ECG recording was performed using lead II configuration (electrode placement), in which the needle electrodes were placed subcutaneously; the negative electrode in the right forelimb; the ground electrode in the right hindlimb; and the positive electrode in the left hindlimb. ECG was recorded in a dimly lit, quiet procedure room. A steady heart rate within the typical mouse range was monitored to ensure that the appropriate anesthetic depth was reached. In order to eliminate circadian influences, ECG was recorded during the morning when the resting phase of a mouse begins. ECG data were collected for up to 120 s and the resulting data analyzed using LabChart software (ADInstruments). The P, Q, R, S and T markers were identified and adjusted as follows: P Start was positioned immediately before the P-wave dip, P Peak was identified as the highest point of the P wave, and P End was marked where the P wave returned to baseline. QRS Start was placed immediately before the QRS wave dip, QRS Max was designated as the highest point of the QRS wave, and QRS End was located between the lowest amplitude of the QRS wave and the J-wave. ST Height was fixed 10 msec from QRS Max. T Peak was determined as the highest or lowest point of the T wave, depending on its polarity, and T End was marked where the T wave returned to baseline, falling between T Peak and P Start. If T End was not visible, the Maximum RT was adjusted in the settings. The QT intervals were also corrected as QTc using the following "Bazett" method: $QTc = QT/(RR/100)^{0.5}$.

4.10. Surgery for electrophysiology

For long-duration electrophysiological local field potential (LFP) recordings of brain activity, 5- to 6-week-old (male and female) B6C3.*Atp1a3* $^{D801N/+}$ (D801N) ($N = 7$), and B6C3.*Atp1a3* $^{E815K/+}$ (E815K) ($N = 11$) and B6C3.*Atp1a3* $^{+/+}$ (wild type) ($N = 5$ for each strain; data were combined in the analyses) mice underwent surgery under isoflurane anesthesia (induction 4 %; maintenance 1.5 %) with oxygen air enrichment and body temperature maintained at 37 ± 0.5 °C. LFP electrodes (75 µm platinum(Pl)/iridium(Ir); PT6718; Advent Research Materials, Oxford, UK) were implanted in the following configuration (in mm relative to bregma, anterior/lateral/ventral, respectively; see also schematic in Fig. 3A): bilateral visual cortex (V1: −3.5/2.0/−0.5), bilateral dorsal hippocampus (dHC: −2.0/1.5/−1.3) and unilateral (right) motor cortex (M1: +1.5/1.8/−0.5). For all operated mice, two low-impedance 75 µm Pt/Ir electrodes with ~1 mm uninsulated tip were also placed in the cerebellum, as reference and ground. All electrode locations were post hoc histologically verified. The recording electrodes were connected to a 7-channel pedestal (E363/0 socket contacts and MS373 pedestal; Plastics One, Roanoke, VA, USA) and connected to the skull using dental cement (075794; Sun Medical SuperBond C&B with L-polymer; Hofmeester, The Netherlands). Carprofen (5 mg/kg, s.c.) was given for post-operative pain relief. All mice survived the surgical procedure and showed no discomfort from surgery during recovery.

4.11. Long-duration local field potential recordings

Following a post-surgery recovery of at least 24 h, the mice were transferred to shielded EEG recording cages in which animals could behave freely. Mice were connected to the EEG system at 6, 10 and 14 weeks of age and recorded for 3–5 days at each given age. The system consisted of a Faraday cage, in which the mouse was connected to custom-built recording hardware via a custom-made counterbalanced, low-torque commutator. LFP recordings were 3× pre-amplified, filtered and fed into separate amplifiers for direct current (DC)-potential (10× gain, relative to reference; DC-500 Hz) and alternating current (AC)-potential signals (200× gain for hippocampal and 400× gain for cortical recordings, relative to reference; 0.05–500 Hz). Recordings were digitized (Power 1401 and Spike2 software, CED, Cambridge, UK) at a sampling rate of 1000 Hz for the DC-potential and at 5000 Hz for AC-potential signals.

4.12. Electrophysiological data analysis

Electrophysiological AC-LFP recordings and DC-potentials were analyzed off-line using Spike2 software (CED, Cambridge, UK), and custom-written Python and MATLAB scripts. To assess spiking activity including spike-wave discharges (SWDs), isolated hippocampal spikes, and giant spikes, AC-potential signals of LFP recordings from cortex (V1 and M1) and hippocampus in a 24-h window were analyzed. The window started at least 24 h after the start of the recording to avoid novelty or stress-induced changes related to connecting the mouse to the EEG recording system. AC-potential LFP recordings were artifact-rejected, band-pass-filtered (0.5–100 Hz) and down-sampled to 1000 Hz. Spike-wave discharges (SWDs) were quantified from the frontal M1 LFP channels based on previous criteria (Kros et al., 2015; Letts et al., 2014). In short, after automatic spike detection, a SWD was defined as an asymmetric complex of at least 3 cycles of sharp negative-positive going spikes and waves with peak-to-peak amplitudes at least two-fold higher than background, a minimal discharge frequency of 6 Hz, a minimal duration of 1 s and inter-SWD episode interval ≥ 1 s. To detect hippocampal isolated spikes and giant spikes, first, an automatic spike detection method was employed using the Nonlinear Energy Operator (NEO) combined with Automatic NEO Thresholding (Yang and Mason, 2017), after which hippocampal giant spikes were identified and extracted from the total number of spikes. Giant spikes were defined as simultaneous spike (either positive or negative) present in all channels, with a large amplitude (> ±10 SD from the filtered baseline) in at least one hippocampal channel, followed by positive deflection ('after hyperpolarization') lasting >200 ms across all channels (Gureviciene et al., 2019). Next, the remaining detected hippocampal spikes were classified as 'isolated hippocampal spikes' based on their features fitting the criterion of a negative-going brief (< 100 ms) single spike, without a corresponding spike within a ± 100-ms window in either the contralateral hippocampus or cortex. The frequency of SWDs, isolated hippocampal spikes and giant spikes was reported as the number of events per hour across a 24-h period of LFP recording, without correlating the data to specific vigilance states.

To assess the occurrence of spontaneous cortical and hippocampal spreading depolarization (SD) events, the entire period of available LFP recordings was analyzed. Cortical or hippocampal SD events were defined in DC-potential recordings as transient negative DC shifts with an amplitude >5 mV, detected with a subsequent delay between at least two LFP recording electrodes associated with a suppression in AC amplitude as visible in the AC-LFP sonogram. Burst spiking activity preceding SD events was defined as high-amplitude (> 2× value of averaged baseline root mean square of the AC-LFP signal) rhythmic discharges that clearly represented an abnormal EEG pattern (typically consisting of repetitive high-amplitude spikes and slow waves), lasting for ≥5 s, followed by suppression of AC-LFP activity. The duration of burst activity was determined from the dorsal HC burst by measuring the

interval between the first and last spike of a burst. Intra-burst spiking frequency was calculated by dividing the total number of spikes by the duration of the burst. SD amplitude was quantified through identifying the lowest of the depolarization during the SD shift, while the 50 % SD-recovery time was assessed from the start of the SD (i.e., start of DC-deflection) to the time-point at which the SD shift had recovered to half of its amplitude level.

To assess cortical network activity features including power spectral analysis (PSD) during active and quiet wakefulness, LFP recorded during the morning (6–12 AM), without the presence of SD events, was analyzed. Vigilance state was determined per 5-s epoch using V1 cortical LFP, and the reference signal and locomotor activity were recorded by the infrared motion detection (PIR) sensor. Active wakefulness was defined by a θ-δ power ratio of >2 during epochs containing locomotor activity and/or high variance in the reference signal. Quiet wakefulness was identified by the presence of desynchronized LFP with no locomotor activity and a stable reference signal, in between epochs of active wakefulness. To differentiate quiet wakefulness from in particular non-rapid-eye-movement (NREM) epochs, the latter were determined by the presence of high-amplitude δ activity indicative of slow-wave-sleep. When quiet wakefulness lasted >20 s and transitioned into NREM sleep, the first 20 s were defined as transition states (i.e., wakefulness to sleep) and not included in the analysis. Attention was given to excluding any large artifact-related activity that could influence the LFP recordings, ensuring accurate assessment of vigilance states. When there was doubt about a sleep - awake period, video footage was used for validation. Next, epochs identified for active and quiet wakefulness were screened for noise deflection and spike exclusion. In total, 5 min of spike-free randomly selected epochs during active and quiet wakefulness were used for θ peak frequency and PSD analysis. Power spectra were computed from V1 cortical LFP by applying a Hamming window over each 5-s epoch, followed by a fast Fourier transform and averaging of the resulting power spectra. For the power comparison of specific frequency bands, oscillations were defined and averaged across the mouse-specific bands: delta (1–5 Hz), theta (5–10 Hz), alpha (10–13 Hz), beta (13–30 Hz) and gamma (30–100 Hz).

4.13. Tissue collection

Animals were euthanized by CO_2 asphyxiation and tissues were harvested, frozen on dry-ice, and stored in the −80 °C freezer until use.

4.14. Detection of Na^+/K^+ ATPase activity and western blotting

Hippocampal tissues from naïve 10-week-old B6C3.*Atp1a3* $^{+/+}$ (wild type), B6C3.*Atp1a3* $^{D801N/+}$ (D801N), and B6C3.*Atp1a3* $^{E815K/+}$ mice (E815K) were homogenized in a buffer of 315 mM sucrose, 20 mM Tris, 1 mM EDTA, pH 7.4, supplemented with complete mini protease inhibitor cocktail (Roche Diagnostics GmBH, Germany). Protein concentrations in crude membrane homogenates were determined with the Lowry method. Gel electrophoresis was performed using mPage 4–12 % MES SDS gels (Millipore, USA) followed by transfer onto nitrocellulose membranes (Bio-Rad, USA). Blots were probed with the mouse monoclonal anti-ATP1A3 (α3) antibody F-1 (sc-374050, Santa Cruz Biotechnology, USA). Anti-GAPDH-HRP antibody (#8884, Cell Signaling Technology, USA) was used as loading control (Supplementary file 8). Signals were developed with WesternBright ECL reagents (Advansta, USA) and quantified with a GE Healthcare LAS 4000 imaging system and ImageQuant software.

ATPase activity was determined by quantifying hydrolysis of ATP. In order to open vesicular structures formed during homogenization, crude membrane homogenates were pre-treated with SDS (final detergent: sample protein ratio of 0.58). The Na^+/K^+-ATPase is resistant to denaturing effects of SDS at this ratio. BSA was added to the solution in order to buffer the exposure to detergent (Sweadner, 2016). Briefly, hippocampi homogenates were preincubated with SDS for 10 min at room temperature in a solution containing 2.0 mg/ml BSA. The reaction was stopped by the addition of three volumes of a solution containing 0.3 mg/ml BSA and no additional detergent. The final ATPase reaction mixture contained 140 mM NaCl, 20 mM KCl, 4 mM MgCl2, 3 mM disodium ATP (Sigma, vanadate free), 30 mM histidine, pH 7.2, in the presence of different concentrations of ouabain, the specific inhibitor of Na^+/K^+-ATPase (Millipore-Sigma). The reaction was incubated for 15 min at 37 °C, followed by quenching with acid-molybdate and addition of Fiske-Subbarow reducing reagent. The developed colour was read at 700 nm. The reaction was performed either in duplicate or triplicate. Na^+/K^+-ATPase due to ATP1A3 (α3) was defined as the difference between total activity with no inhibitor added and the one inhibited by 10 μM ouabain, whereas activity due to ATP1A1 (α1) as that active in 10 μM ouabain but inhibited by 3 mM ouabain. The data are expressed as μmol of inorganic phosphate released by 1 mg of total protein in an hour (μmol/mg/h). There are three isoforms of catalytic subunit of Na^+/K^+-ATPase in brain. α1 is expressed widely, whereas ATP1A2 (α2) and ATP1A3 (α3) are specific for glia and neurons, respectively. Activity conferred by ATP1A2 (α2) is no more than 5–10 % of the total activity and it may be ignored (Liu et al., 2024). In rodents, α1 and α2 + α3 isoforms differ in their sensitivity to ouabain and this allows separation of effects on ATPase activity conferred by α1 and α2 + α3 isoforms (Fig. 1C) (Loreaux et al., 2008; O'Brien et al., 1994; Price and Lingrel, 1988). Most of the Na^+/K^+-ATPase activity recovered from hippocampal samples came from the α3 isoform. Quantifications were performed using mice of either sex.

4.15. Reverse transcription and quantitative PCR (TaqMan) analysis

Mouse tissues (cortex, hippocampus, brainstem and cerebellum) were collected from naïve 10-week-old B6C3.*Atp1a3* $^{+/+}$ (wild type), B6C3.*Atp1a3* $^{D801N/+}$ (D801N), and B6C3.*Atp1a3* $^{E815K/+}$ mice (E815K) with four biological replicates per genotype and brain region. The RNA was isolated using RNeasy Mini Kit and DNase-treated following the manufacturer's protocol (Qiagen) and was used for cDNA synthesis using High-Capacity cDNA Reverse Transcription Kit and oligo dT primer (ThermoFisher) as per the manufacturer's protocol. Quantitative RT-PCR (TaqMan) reactions were performed using the Taqman Fast Advance MasterMix (ThermoFisher) and the QuantStudio Flex 7 qPCR detection system (ThermoFisher). For quantitative expression analysis, TaqMan probes (see table below) were multiplexed with probes for the gene of interest and input control (*Tata-binding protein, Tbp*). The expression levels of the gene of interest (FAM) were normalized to those of *Tbp* (HEX) using the 2-ΔΔCT method (Livak and Schmittgen, 2001) and expressed as the fold change ± standard error of the mean (SEM) relative to wild type. Quantifications were performed using mice of either sex.

TaqMan Probes:

Gene name	Species	Exon location	Fluorophore	Vendor	Cat. number
Bmp3	Mouse	2–3	FAM	IDT	Mm. PT.58.11601208
Olfm4	Mouse	2–3	FAM	IDT	Mm. PT.58.14228836
Htra4	Mouse	3–4	FAM	IDT	Mm. PT.56a.6274186
Rara	Mouse	6–7	FAM	IDT	Mm. PT.58.11675696
Crhr2	Mouse	6–7	FAM	IDT	Mm. PT.58.12499462
Th	Mouse	12–13	FAM	IDT	Mm. PT.58.33106186
Itgax	Mouse	5–6	FAM	IDT	Mm. PT.58.42516719
Car9	Mouse	1–3	FAM	IDT	Mm. PT.58.14228651
Tbp	Mouse	4–5	HEX	IDT	Mm. PT.39a.22214839

4.16. RNA sequencing library construction

Mouse tissues (cortex, hippocampus, brainstem and cerebellum) were collected from naïve 10-week-old B6C3.*Atp1a3* $^{+/+}$ (wild type), B6C3.*Atp1a3* $^{D801N/+}$ (D801N), and B6C3.*Atp1a3* $^{E815K/+}$ mice (E815K) to obtain four (2 female and 2 male mice) biological replicates per genotype and brain region. The RNA was isolated using RNeasy Mini Kit and DNase-treated following the manufacturer's protocol (Qiagen) and used for RNA library construction as per the manufacturer's protocol (KAPA mRNA HyperPrep Kit, Roche Sequencing and Life Sciences). Briefly, the protocol includes isolation of polyA containing mRNA using oligo-dT magnetic beads, RNA fragmentation, first and second strand cDNA synthesis, ligation of Illumina-specific adapters containing a unique barcode sequence for each library, and PCR amplification. The quality and concentration of the libraries were assessed using the D5000 ScreenTape (Agilent Technologies) and Qubit dsDNA HS Assay (ThermoFisher), respectively. All libraries were pooled (48 samples), and the pool was sequenced as paired end (150 bp) on an Illumina NovaSeq X Plus using the 10B Reagent Kit with a target of at least 30 million reads per sample.

4.17. Analysis of RNA sequencing data

First, adapters were trimmed from read pairs using cutadapt (Martin, 2011) version 4.4 using parameters -a AGATCGGAAGAGCACACGT CTGAACTCCAGTCA, -A AGATCGGAAGAGCGTCGTGTAGGGAAAGAGT GT and -m 40. Trimmed reads were used to quantify expression with kallisto version 0.48.0 (Bray et al., 2016) by pseudo-aligning to a GENCODE version M35 reference transcriptome (with –bias parameter set). The resulting transcript abundance estimates were imported into R using tximport (Soneson et al., 2015) for differential expression analysis using DESeq2 version 1.38.3 (Love et al., 2014). For each tissue, expression of B6C3.*Atp1a3* $^{D801N/+}$ (D801N) or B6C3.*Atp1a3* $^{E815K/+}$ mice was compared to expression of B6C3.*Atp1a3* $^{+/+}$ (wild type) using a linear model including sex as a covariate and testing for differences in genotype. Fold change was estimated using an adaptive shrinkage estimator from the ahsr (version 2.2–65) R package (Stephens, 2017).

4.18. Pathway analysis

Gene expression data were analyzed using Ingenuity Pathway Analysis (IPA, QIAGEN Inc., https://www.qiagenbioinformatics.com/products/ingenuity-pathway-analysis). Kyoto Encyclopedia of Genes and Genomes (KEGG) pathway analysis was performed using the ShinyGO v0.61 bioinformatics web server (http://bioinformatics.sdstate.edu/go) (Ge et al., 2020) by uploading the gene lists from our RNA sequencing analysis. KEGG pathway terms with a *p*-value cutoff (FDR) $\leq$ 0.05 were considered enriched.

4.19. Histology and immunohistochemistry

Mice were transcardially perfused with PBS and then with 10 % Neutral buffered formalin (NBF) for immunohistochemistry (IHC). Brain tissues were post-fixed (24–48 h) in NBF and then embedded in paraffin. For IHC staining, sections were deparaffinized, rehydrated, and the NBF-fixed, paraffin embedded sections were stained with antibodies against GFAP (Abcam 16997, 1:100, antigen retrieval via citrate buffer for 20 min) and Iba1 (Abcam 178846, 1:2000, antigen retrieval via citrate buffer for 5 min) on the Leica-Bond auto-staining system (Leica Biosystems). Sections were counterstained with Hematoxylin and histological slides were digitalized at 40× resolution using a digital slide scanner (Hamamatsu NanoZoomer). For GFAP and Iba1 quantification, the staining intensity was measured in an area of 0.3 mm^2 (somatosensory cortex, layer I to VI), 0.09 mm^2 (CA1 of hippocampus), 0.5 mm^2 (thalamus), and 0.1 mm^2 (DCN of the cerebellum) using ImageJ, averaged from three parasagittal brain sections (three brain sections spaced 150 μm apart) per animal and expressed as the fold change relative to wild type mice per strain and brain region. Quantifications were performed using mice of either sex.

4.20. Serum collection and NFL analysis

Whole blood was collected via retro-orbital collection (RO) after applying a topical anesthetic (Proparacaine) on the eye. The collected blood was transferred into the serum collection tube (Microtainer Tube with serum separator, yellow cap), the tube was inverted a few times, kept at room temperature for 20–30 min, stored on wet-ice and then, centrifuged for 10 min at 14,000 x g (rcf) at 4 °C. Afterwards, the serum located above the gel separator matrix was transferred into a new storage tube and stored at −80 °C until further analysis. Serum samples were subjected to neurofilament light chain (NFL) analysis with a 32× sample dilution and 2 replicates (technical replicates) per sample via Simoa HD-X analyzer (Simoa NF-Light v2 Advantage Kit #104073 by Quanterix). Quantifications were performed using mice of either sex.

4.21. Statistics

For quantification of RNA expression (TaqMan), ATPase activity and protein expression, mouse behavioral data, serum NFL levels, and histological quantifications, *p*-values were computed in GraphPad Prism or RStudio using either student's *t*-test, Mantel-Cox test, Fisher's exact test, multiple *t*-tests, one-way ANOVA, or two-way ANOVA and statistical tests were corrected for multiple comparisons as indicated in the figure legends. Quantifications were performed with mice of either sex. The number of biological replicates is depicted in each figure throughout the manuscript. For behavioral (e.g., HIP, rotarod, open field, grip strength and ECG) and molecular (e.g., NFL, TaqMan, IHC) analysis, operators were blinded during testing, data collection and analysis. For the analysis of RNA sequencing and electrophysiology data, operators were unblinded as the identification of changes and abnormalities required knowledge of the respective genotypes. Except for the survival curves, behavioral data are shown as the pool of 'male + female' mice because the absence or presence of significant changes were independent of sex.

Supplementary data to this article can be found online at https://doi.org/10.1016/j.nbd.2025.106954.

CRediT authorship contribution statement

Markus Terrey: Writing – review & editing, Writing – original draft, Visualization, Validation, Supervision, Project administration, Methodology, Investigation, Formal analysis, Data curation, Conceptualization. **Georgii Krivoshein:** Writing – review & editing, Visualization, Investigation, Formal analysis, Data curation. **Scott I. Adamson:** Writing – review & editing, Software, Formal analysis, Data curation. **Elena Arystarkhova:** Writing – review & editing, Investigation, Formal analysis, Data curation. **Laura Anderson:** Writing – review & editing, Project administration, Formal analysis, Data curation. **John Szwec:** Formal analysis. **Shelby McKee:** Formal analysis. **Holly Jones:** Formal analysis. **Sara Perkins:** Formal analysis. **Vijay Selvam:** Formal analysis. **Pierre-Alexandre Piec:** Formal analysis. **Dweet Chhaya:** Formal analysis. **Ari Dehn:** Formal analysis. **Aamir Zuberi:** Resources, Methodology. **Stephen A. Murray:** Resources, Funding acquisition. **Natalia S. Morsci:** Writing – review & editing, Methodology, Conceptualization. **Kathleen J. Sweadner:** Writing – review & editing, Supervision, Formal analysis, Data curation, Conceptualization. **David A. Knowles:** Writing – review & editing, Supervision. **Else A. Tolner:** Writing – review & editing, Supervision, Investigation, Formal analysis, Data curation. **Arn M.J.M. van den Maagdenberg:** Writing – original draft, Supervision, Resources, Investigation, Funding acquisition, Data curation. **Cathleen**

M. Lutz: Writing – review & editing, Supervision, Resources, Investigation, Funding acquisition.

Funding

This work was supported by the Chan-Zuckerberg Initiative (EA and KJS; PI David R. Liu), the Dutch National Epilepsy Foundation (2022-10; EAT and AMJMvdM), the European Union Joint Programme Neurodegenerative Disease Research project (REBALANCE, 10510062210003; EAT and AMJMvdM), the Medical Delta program "Medical NeuroDelta: Ambulant Neuromonitoring for Prevention and Treatment of Brain Disease" (AMJMvdM), the Center for Precision Genetics at The Jackson Laboratory (NIH grant U54 OD030187, CML), and the Mouse Mutant Resource and Research Center (NIH grant U42 OD010921, CML).

Declaration of competing interest

The authors declare no competing interests.

Acknowledgements

We thank the patients and family members of the AHC patient advocacy groups including Nina Frost (Hope for Annabel), Mary Saladino (For Henry), Simon Frost (Cure AHC), Vicky Platt and Stephen Henderson (AHC foundation) for their support and providing the patient perspectives. We thank Dr. Mohamad A. Mikati for sharing the 'Matb' (Atp1a3 tm1.1Mika) mice. We thank Drs. Kathryn J. Swoboda, Hendrick Rosewich, Matthew Campbell, Alfred L. George, Christine Q. Simmons, Steven J. Clapcote, Nutan Sharma, Laurie Ozelius, David R. Liu, Alexander A. Sousa, and Holt A. Sakai for their clinical and ATP1A3-related research expertise, and valuable discussions. We thank Dr. David R. Liu for supporting the biochemical AHC studies. We thank the Scientific Services at the Jackson Laboratory (JAX) including the Mouse Model Generation Core, Reproductive Sciences, Genome Technologies, Center for Biometric Analysis, Clinical Chemistry, Histology and Microscopy Cores for their support with the *in vitro* fertilization, RNA-sequencing, behavioral test equipment, serum NFL analysis, histology and microscopy equipment. We thank the DIVA (Digital In Vivo Alliance) consortium for the access to the digital cage system. We thank all RDTC (Rare Disease Translational Center) and JCPG (JAX Center for Precision Genetics) members for their operational support.

Data availability

The RNA sequencing data have been deposited to GEO with the identifier (GSE279074). Details about the sample and sequencing inventory have been provided (see Supplementary file 6 - Sample Sequencing log). Codes for the RNA Sequencing data analysis, quality control, and data processing have been made available at https://github.com/scottiadamson/atp1a3_mouse_rna_seq_analysis

References

Adamu, A., Li, S., Gao, F., Xue, G., 2024. The role of neuroinflammation in neurodegenerative diseases: current understanding and future therapeutic targets. Front. Aging Neurosci. 16, 1–16. https://doi.org/10.3389/fnagi.2024.1347987.

Aiba, I., Noebels, J.L., 2015. Spreading depolarization in the brainstem mediates sudden cardiorespiratory arrest in mouse SUDEP models. Sci. Transl. Med. 7, 282ra46. https://doi.org/10.1126/scitranslmed.aaa4050.

Aïssa, H.B., Sala, R.W., Georgescu Margarint, E.L., Frontera, J.L., Varani, A.P., Menardy, F., Pelosi, A., Hervé, D., Léna, C., Popa, D., 2022. Functional abnormalities in the cerebellothalamic pathways in a mouse model of DYT25 dystonia. Elife 11. https://doi.org/10.7554/eLife.79135.

Amalia, L., 2021. Glial fibrillary acidic protein (GFAP): Neuroinflammation biomarker in acute ischemic stroke. J. Inflamm. Res. 14, 7501–7506. https://doi.org/10.2147/JIR.S342097.

Arystarkhova, E., Haq, I.U., Luebbert, T., Mochel, F., Saunders-Pullman, R., Bressman, S. B., Feschenko, P., Salazar, C., Cook, J.F., Demarest, S., Brashear, A., Ozelius, L.J., Sweadner, K.J., 2019. Factors in the disease severity of ATP1A3 mutations: impairment, misfolding, and allele competition. Neurobiol. Dis. 132, 104577. https://doi.org/10.1016/j.nbd.2019.104577.

Arystarkhova, E., Ozelius, L.J., Brashear, A., Sweadner, K.J., 2021. Misfolding, altered membrane distributions, and the unfolded protein response contribute to pathogenicity differences in Na,K-ATPase ATP1A3 mutations. J. Biol. Chem. 296, 100019. https://doi.org/10.1074/jbc.RA120.015271.

Azarias, G., Kruusmägi, M., Connor, S., Akkuratov, E.E., Liu, X.L., Lyons, D., Brismar, H., Broberger, C., Aperia, A., 2013. A specific and essential role for Na,K-ATPase α3 in neurons co-expressing α1 and α3. J. Biol. Chem. 288, 2734–2743. https://doi.org/10.1074/jbc.M112.425785.

Bacioglu, M., Maia, L.F., Preische, O., Schelle, J., Apel, A., Kaeser, S.A., Schweighauser, M., Eninger, T., Lambert, M., Pilotto, A., Shimshek, D.R., Neumann, U., Kahle, P.J., Staufenbiel, M., Neumann, M., Maetzler, W., Kuhle, J., Jucker, M., 2016. Neurofilament Light chain in blood and CSF as marker of disease progression in mouse models and in neurodegenerative diseases. Neuron 91, 56–66. https://doi.org/10.1016/j.neuron.2016.05.018.

Baladron, J., Vitay, J., Fietzek, T., Hamker, F.H., 2023. The contribution of the basal ganglia and cerebellum to motor learning: a neurocomputational approach. PLoS Comput. Biol. 19, 1–29. https://doi.org/10.1371/journal.pcbi.1011024.

Balestrini, S., Mikati, M.A., Álvarez-García-Rovés, R., Carboni, M., Hunanyan, A.S., Kherallah, B., McLean, M., Prange, L., De Grandis, E., Gagliardi, A., Pisciotta, L., Stagnaro, M., Veneselli, E., Campistol, J., Fons, C., Pias-Peleteiro, L., Brashear, A., Miller, C., Samões, R., Brankovic, V., Padiath, Q.S., Potic, A., Pilch, J., Vezyroglou, A., Bye, A.M.E., Davis, A.M., Ryan, M.M., Semsarian, C., Hollingsworth, G., Scheffer, I.E., Granata, T., Nardocci, N., Ragona, F., Arzimanoglou, A., Panagiotakaki, E., Carrilho, I., Zucca, C., Novy, J., Dzieżyc, K., Parowicz, M., Mazurkiewicz-Bełdzińska, M., Weckhuysen, S., Pons, R., Groppa, S., Sinden, D.S., Pitt, G.S., Tinker, A., Ashworth, M., Michalak, Z., Thom, M., Cross, J.H., Vavassori, R., Kaski, J.P., Sisodiya, S.M., 2020. Cardiac phenotype in ATP1A3-related syndromes: a multicenter cohort study. Neurology 95, e2866–e2879. https://doi.org/10.1212/WNL.0000000000010794.

Barro, C., Chitnis, T., Weiner, H.L., 2020. Blood neurofilament light: a critical review of its application to neurologic disease. Ann. Clin. Transl. Neurol. 7, 2508–2523. https://doi.org/10.1002/acn3.51234.

Bavato, F., Barro, C., Schnider, L.K., Simrén, J., Zetterberg, H., Seifritz, E., Quednow, B. B., 2024. Introducing neurofilament light chain measure in psychiatry: current evidence, opportunities, and pitfalls. Mol. Psychiatry. https://doi.org/10.1038/s41380-024-02524-6.

Bervoets, S., Wei, N., Erfurth, M.L., Yusein-Myashkova, S., Ermanoska, B., Mateiu, L., Asselbergh, B., Blocquel, D., Kakad, P., Penserga, T., Thomas, F.P., Guergueltcheva, V., Tournev, I., Godenschwege, T., Jordanova, A., Yang, X.L., 2019. Transcriptional dysregulation by a nucleus-localized aminoacyl-tRNA synthetase associated with Charcot-Marie-tooth neuropathy. Nat. Commun. 10. https://doi.org/10.1038/s41467-019-12909-9.

Beyer, B., Deleuze, C., Letts, V.A., Mahaffey, C.L., Boumil, R.M., Lew, T.A., Huguenard, J. R., Frankel, W.N., 2008. Absence seizures in C3H/HeJ and knockout mice caused by mutation of the AMPA receptor subunit Gria4. Hum. Mol. Genet. 17, 1738–1749. https://doi.org/10.1093/hmg/ddn064.

Birchler, J.A., Yao, H., Chudalayandi, S., 2006. Unraveling the genetic basis of hybrid vigor. Proc. Natl. Acad. Sci. U. S. A. 103, 12957–12958. https://doi.org/10.1073/pnas.0605627103.

Boonsimma, P., Michael Gasser, M., Netbaramee, W., Wechapinan, T., Srichomthong, C., Ittiwut, C., Wagner, M., Krenn, M., Zimprich, F., Abicht, A., Biskup, S., Roser, T., Borggraefe, I., Suphapeetiporn, K., Shotelersuk, V., 2020. Mutational and phenotypic expansion of ATP1A3-related disorders: report of nine cases. Gene 749, 144709. https://doi.org/10.1016/j.gene.2020.144709.

Bray, N.L., Pimentel, H., Melsted, P., Pachter, Lior, 2016. Near-optimal probabilistic RNA-seq quantification. Nat. Biotechnol. 34, 525–527. https://doi.org/10.1038/nbt.3519.

Buzsáki, G., 2015. Hippocampal sharp wave-ripple: a cognitive biomarker for episodic memory and planning. Hippocampus 25, 1073–1188. https://doi.org/10.1002/hipo.22488.

Cao, S., Fisher, D.W., Rodriguez, G., Yu, T., Dong, H., 2021. Comparisons of neuroinflammation, microglial activation, and degeneration of the locus coeruleus-norepinephrine system in APP/PS1 and aging mice. J. Neuroinflammation 18, 1–16. https://doi.org/10.1186/s12974-020-02054-2.

Capuano, A., Garone, G., Tiralongo, G., Graziola, F., 2020. Alternating hemiplegia of childhood: understanding the genotype–phenotype relationship of ATP1A3 variations. Appl. Clin. Genet. 13, 71–81. https://doi.org/10.2147/TACG.S210325.

Carlson, G.A., Borchelt, D.R., Dake, A., Turner, S., Danielson, V., Coffin, J.D., Eckman, C., Meiners, J., Nilsen, S.P., Younkin, S.G., Hsiao, K.K., 1997. Genetic modification of the phenotypes produced by amyloid precursor protein overexpression in transgenic mice. Hum. Mol. Genet. 6, 1951–1959. https://doi.org/10.1093/hmg/6.11.1951.

Carter, M., Shieh, J., 2015. Chapter 2 - animal behavior. In: Carter, M., Shieh, J. (Eds.), Guide to Research Techniques in Neuroscience, Second edition. Academic Press, San Diego, pp. 39–71. https://doi.org/10.1016/B978-0-12-800511-8.00002-2.

Chan, J.C., Houghton, A.B., Bale, T.L., 2017. Strained in planning your mouse background? Using the HPA stress Axis as a biological readout for backcrossing strategies. Neuropsychopharmacology 42, 1749–1751. https://doi.org/10.1038/npp.2017.66.

Chauhan, P., Philip, S., Chauhan, G., 2022. The Anatomical Basis of Seizures. Epilepsy. https://doi.org/10.36255/exon-publications-epilepsy-anatomical-basis.

Chiu, I.M., Morimoto, E.T.A., Goodarzi, H., Liao, J.T., O'Keeffe, S., Phatnani, H.P., Muratet, M., Carroll, M.C., Levy, S., Tavazoie, S., Myers, R.M., Maniatis, T., 2013. A neurodegeneration-specific gene-expression signature of acutely isolated microglia

from an amyotrophic lateral sclerosis mouse model. Cell Rep. 4, 385–401. https://doi.org/10.1016/j.celrep.2013.06.018.
Clapcote, S.J., Duffy, S., Xie, G., Kirshenbaum, G., Bechard, A.R., Schack, V.R., Petersen, J., Sinai, L., Saab, B.J., Lerch, J.P., Minassian, B.A., Ackerley, C.A., Sled, J. G., Cortez, M.A., Henderson, J.T., Vilsen, B., Roder, J.C., 2009. Mutation I810N in the α3 isoform of Na+,K +-ATPase causes impairments in the sodium pump and hyperexcitability in the CNS. Proc. Natl. Acad. Sci. U. S. A. 106, 14085–14090. https://doi.org/10.1073/pnas.0904817106.
Cording, K.R., Bateup, H.S., 2023. Altered motor learning and coordination in mouse models of autism spectrum disorder. Front. Cell. Neurosci. 17, 1–18. https://doi.org/10.3389/fncel.2023.1270489.
De Carvalho Aguiar, P., Sweadner, K.J., Penniston, J.T., Zaremba, J., Liu, L., Caton, M., Linazasoro, G., Borg, M., Tijssen, M.A.J., Bressman, S.B., Dobyns, W.B., Brashear, A., Ozelius, L.J., 2004. Mutations in the Na+/K+-ATPase α3 gene ATP1A3 are associated with rapid-onset dystonia parkinsonism. Neuron 43, 169–175. https://doi.org/10.1016/j.neuron.2004.06.028.
DeAndrade, M.P., Yokoi, F., van Groen, T., Lingrel, J.B., Li, Y., 2011. Characterization of Atp1a3 mutant mice as a model of rapid-onset dystonia with parkinsonism. Behav. Brain Res. 216, 659–665. https://doi.org/10.1016/j.bbr.2010.09.009.
DiSabato, D.J., Quan, N., Godbout, J.P., 2016. Neuroinflammation: the devil is in the details. J. Neurochem. 139 (Suppl), 136–153. https://doi.org/10.1111/jnc.13607.
Dobretsov, M., Hayar, A., Kockara, N.T., Kozhemyakin, M., Light, K.E., Patyal, P., Pierce, D.R., Wight, P.A., 2019. A Transgenic Mouse Model to Selectively Identify α 3 Na,K-ATPase Expressing Cells in the Nervous System. Neuroscience 398, 274–294. https://doi.org/10.1016/j.neuroscience.2018.07.018.
Drinkenburg, W.H.I.M., Ahnaou, A., Ruigt, G.S.F., 2015. Pharmaco-EEG studies in animals: a history-based introduction to contemporary translational applications. Neuropsychobiology 72, 139–150. https://doi.org/10.1159/000443175.
Du, M., Li, J., Chen, L., Yu, Y., Wu, Y., 2018. Astrocytic Kir4.1 channels and gap junctions account for spontaneous epileptic seizure. PLoS Comput. Biol. 14, 1–19. https://doi.org/10.1371/journal.pcbi.1005877.
Duchon, A., Pothion, S., Brault, V., Sharp, A.J., Tybulewicz, V.L.J., Fisher, E.M.C., Herault, Y., 2011. The telomeric part of the human chromosome 21 from Cstb to Prmt2 is not necessary for the locomotor and short-term memory deficits observed in the Tc1 mouse model of down syndrome. Behav. Brain Res. 217, 271–281. https://doi.org/10.1016/j.bbr.2010.10.023.
Eyo, U.B., Peng, J., Swiatkowski, P., Mukherjee, A., Bispo, A., Wu, L.J., 2014. Neuronal hyperactivity recruits microglial processes via neuronal NMDA receptors and microglial P2Y12 receptors after status epilepticus. J. Neurosci. 34, 10528–10540. https://doi.org/10.1523/JNEUROSCI.0416-14.2014.
Eyo, U.B., Murugan, M., Wu, L.J., 2017. Microglia–Neuron Communication in Epilepsy. Glia 65, 5–18. https://doi.org/10.1002/glia.23006.
Foiadelli, T., Santangelo, A., Costagliola, G., Costa, E., Scacciati, M., Riva, A., Volpedo, G., Smaldone, M., Bonuccelli, A., Clemente, A.M., Ferretti, A., Savasta, S., Striano, P., Orsini, A., 2023. Neuroinflammation and status epilepticus: a narrative review unraveling a complex interplay. Front. Pediatr. 11, 1–12. https://doi.org/10.3389/fped.2023.1251914.
Foltz, C.J., Ullman-Cullere, M., 1999. Guidelines for assessing the health and condition of mice. Lab Anim. (NY). 28, 28–32.
Ford, C.P., Littlejohn, R.O., German, R., Vuocolo, B., Aceves, J., Vossaert, L., Owen, N., Wangler, M., Schmid, C.A., 2023. Precision therapy for a medically actionable ATP1A3 variant from a genomic medicine program in an underserved population. Mol. Genet. Genomic Med. 11, 1–6. https://doi.org/10.1002/mgg3.2272.
Frankel, W.N., Beyer, B., Maxwell, C.R., Pretel, S., Letts, V.A., Siegel, S.J., 2005. Development of a new genetic model for absence epilepsy: spike-wave seizures in C3H/He and backcross mice. J. Neurosci. 25, 3452–3458. https://doi.org/10.1523/JNEUROSCI.0231-05.2005.
Frankel, W.N., Mahaffey, C.L., McGarr, T.C., Beyer, B.J., Letts, V.A., 2014. Unraveling genetic modifiers in the Gria4 mouse model of absence epilepsy. PLoS Genet. 10. https://doi.org/10.1371/journal.pgen.1004454.
Freedman, M.S., Gnanapavan, S., Booth, R.A., Calabresi, P.A., Khalil, M., Kuhle, J., Lycke, J., Olsson, T., 2024. Guidance for use of neurofilament light chain as a cerebrospinal fluid and blood biomarker in multiple sclerosis management. eBioMedicine 101, 104970. https://doi.org/10.1016/j.ebiom.2024.104970.
Fujii, F., Kanemasa, H., Okuzono, S., Setoyama, D., Taira, R., Yonemoto, K., Motomura, Y., Kato, H., Masuda, K., Kato, T.A., Ohga, S., Sakai, Y., 2024. ATP1A3 regulates protein synthesis for mitochondrial stability under heat stress. DMM Dis. Model. Mech. 17. https://doi.org/10.1242/dmm.050574.
Ge, S.X., Jung, D., Jung, D., Yao, R., 2020. ShinyGO: a graphical gene-set enrichment tool for animals and plants. Bioinformatics 36, 2628–2629. https://doi.org/10.1093/bioinformatics/btz931.
Gokce, O., Stanley, G.M., Treutlein, B., Neff, N.F., Camp, J.G., Malenka, R.C., Rothwell, P.E., Fuccillo, M.V., Südhof, T.C., Quake, S.R., 2016. Cellular taxonomy of the mouse striatum as revealed by single-cell RNA-Seq. Cell Rep. 16, 1126–1137. https://doi.org/10.1016/j.celrep.2016.06.059.
Gravesteijn, G., Rutten, J.W., Verberk, I.M.W., Böhringer, S., Liem, M.K., van der Grond, J., Aartsma-Rus, A., Teunissen, C.E., Lesnik Oberstein, S.A.J., 2019. Serum Neurofilament light correlates with CADASIL disease severity and survival. Ann. Clin. Transl. Neurol. 6, 46–56. https://doi.org/10.1002/acn3.678.
Grillo, E., 2015. Postictal MRI abnormalities and seizure-induced brain injury: notions to be challenged. Epilepsy Behav. 44, 195–199. https://doi.org/10.1016/j.yebeh.2015.01.001.
Gureviciene, I., Ishchenko, I., Ziyatdinova, S., Jin, N., Lipponen, A., Gurevicius, K., Tanila, H., 2019. Characterization of epileptic spiking associated with brain amyloidosis in APP/PS1 mice. Front. Neurol. 10, 1151. https://doi.org/10.3389/fneur.2019.01151.
Hallett, M., 2011. Neurophysiology of dystonia: the role of inhibition. Neurobiol. Dis. 42, 177–184. https://doi.org/10.1016/j.nbd.2010.08.025.
Haq, I.U., Snively, B.M., Sweadner, K.J., Suerken, C.K., Cook, J.F., Ozelius, L.J., Miller, C., McCall, W.V., Whitlow, C.T., Brashear, A., 2019. Revising rapid-onset dystonia-parkinsonism: broadening indications for ATP1A3 testing. Mov. Disord. 34, 1528–1536. https://doi.org/10.1002/mds.27801.
Hawkins, N.A., Dekeyser, J., Kearney Jr., J.A., A.L.G, 2024. Novel mouse model of alternating hemiplegia of childhood exhibits prominent motor and seizure phenotypes. Neurobiol. Dis. 203. https://doi.org/10.1016/j.nbd.2024.106751.
Heinzen, E.L., Swoboda, K.J., Hitomi, Y., Gurrieri, F., De Vries, B., Tiziano, F.D., Fontaine, B., Walley, N.M., Heavin, S., Panagiotakaki, E., Fiori, S., Abiusi, E., Di Pietro, L., Sweney, M.T., Newcomb, T.M., Viollet, L., Huff, C., Jorde, L.B., Reyna, S. P., Murphy, K.J., Shianna, K.V., Gumbs, C.E., Little, L., Silver, K., Ptáček, L.J., Haan, J., Ferrari, M.D., Bye, A.M., Herkes, G.K., Whitelaw, C.M., Webb, D., Lynch, B. J., Uldall, P., King, M.D., Scheffer, I.E., Neri, G., Arzimanoglou, A., Van Den Maagdenberg, A.M.J.M., Sisodiya, S.M., Mikati, M.A., Goldstein, D.B., Koelewijn, S., Kamphorst, J., Geilenkirchen, M., Pelzer, N., Ferrari, M., Van Den Maagdenberg, A., Zucca, C., Franchini, F., Vavassori, R., Giannotta, M., Gobbi, G., Granata, T., Nardocci, N., De Grandis, E., Veneselli, E., Stagnaro, M., Vigevano, F., Oechsler, C., Nicole, S., Ninan, M., Neville, B., Ebinger, F., Fons, C., Campistol, J., Kemlink, D., Nevsimalova, S., Laan, L., Peeters-Scholte, C., Casaer, P., Casari, G., Sange, G., Spiel, G., Boneschi, F.M., Bassi, M.T., Schyns, T., Crawley, F., Poncelin, D., 2012. De novo mutations in ATP1A3 cause alternating hemiplegia of childhood. Nat. Genet. 44, 1030–1034. https://doi.org/10.1038/ng.2358.
Heinzen, E.L., Arzimanoglou, A., Brashear, A., Clapcote, S.J., Gurrieri, F., Goldstein, D.B., Jóhannesson, S.H., Mikati, M.A., Neville, B., Nicole, S., Ozelius, L.J., Poulsen, H., Schyns, T., Sweadner, K.J., van den Maagdenberg, A., Vilsen, B., 2014. Distinct neurological disorders with ATP1A3 mutations. Lancet Neurol. 13, 503–514. https://doi.org/10.1016/S1474-4422(14)70011-0.
Helseth, A.R., Hunanyan, A.S., Adil, S., Linabarger, M., Sachdev, M., Abdelnour, E., Arehart, E., Szabo, M., Richardson, J., Wetsel, W.C., Hochgeschwender, U., Mikati, M.A., 2018. Novel E815K knock-in mouse model of alternating hemiplegia of childhood. Neurobiol. Dis. 119, 100–112. https://doi.org/10.1016/j.nbd.2018.07.028.
Henriksen, C., Kjaer-Sorensen, K., Einholm, A.P., Madsen, L.B., Momeni, J., Bendixen, C., Oxvig, C., Vilsen, B., Larsen, K., 2013. Molecular cloning and characterization of porcine Na+/K +-ATPase isoforms α1, α2, α3 and the ATP1A3 promoter. PloS One 8. https://doi.org/10.1371/journal.pone.0079127.
Herrera, V.L., Cova, T., Sassoon, D., Ruiz-Opazo, N., 1994. Developmental cell-specific regulation of Na(+)-K(+)-ATPase alpha 1-, alpha 2-, and alpha 3-isoform gene expression. Am. J. Physiol. 266, C1301–C1312. https://doi.org/10.1152/ajpcell.1994.266.5.C1301.
Holm, T.H., Lykke-Hartmann, K., 2016. Insights into the pathology of the α3 Na+/K+-ATPase ion pump in neurological disorders; lessons from animal models. Front. Physiol. 7, 1–12. https://doi.org/10.3389/fphys.2016.00209.
Holm, T.H., Isaksen, T.J., Glerup, S., Heuck, A., Bøttger, P., Füchtbauer, E.M., Nedergaard, S., Nyengaard, J.R., Andreasen, M., Nissen, P., Lykke-Hartmann, K., 2016. Cognitive deficits caused by a disease-mutation in the α 3 Na+/K+-ATPase isoform. Sci. Rep. 6, 1–15. https://doi.org/10.1038/srep31972.
Holtman, I.R., Noback, M., Bijlsma, M., Duong, K.N., van der Geest, M.A., Ketelaars, P.T., Brouwer, N., Vainchtein, I.D., Eggen, B.J.L., Boddeke, H.W.G.M., 2015. Glia open access database (GOAD): a comprehensive gene expression encyclopedia of glia cells in health and disease. Glia 63, 1495–1506. https://doi.org/10.1002/glia.22810.
Huangyang, P., Simon, M.C., 2018. Hidden features: exploring the non-canonical functions of metabolic enzymes. Dis. Model. Mech. 11. https://doi.org/10.1242/dmm.033365.
Hunanyan, A.S., Fainberg, N.A., Linabarger, M., Arehart, E., Leonard, A.S., Adil, S.M., Helseth, A.R., Swearingen, A.K., Forbes, S.L., Rodriguiz, R.M., Rhodes, T., Yao, X., Kibbi, N., Hochman, D.W., Wet, W.C., Mohamad, A., Mikati, 2014. Knock-in mouse model of alternating hemiplegia of childhood: Behavioral and electrophysiologic characterization. https://doi.org/10.1111/epi.12878.
Hunanyan, A.S., Helseth, A.R., Abdelnour, E., Kherallah, B., Sachdev, M., Chung, L., Masoud, M., Richardson, J., Li, Q., Nadler, J.V., Moore, S.D., Mikati, M.A., 2018. Mechanisms of increased hippocampal excitability in the Mashl(+/−) mouse model of Na(+) /K(+) -ATPase dysfunction. Epilepsia 59, 1455–1468. https://doi.org/10.1111/epi.14441.
Hunanyan, A.S., Kantor, B., Puranam, R.S., Elliott, C., Mccall, A., Dhindsa, J., Pagadala, P., Wallace, K., Poe, J., Gunduz, T., Asokan, A., Koeberl, D.D., Elmallah, M.K., Mikati, M.A., 2021. Adeno-associated virus-mediated gene therapy in the Mashlool, Atp1a3Mashl/+, mouse model of alternating hemiplegia of childhood. Hum. Gene Ther. 32, 405–419. https://doi.org/10.1089/hum.2020.191.
Ikeda, K., Satake, S., Onaka, T., Sugimoto, H., Takeda, N., Imoto, K., Kawakami, K., 2013. Enhanced inhibitory neurotransmission in the cerebellar cortex of Atp1a3-deficient heterozygous mice. J. Physiol. 591, 3433–3449. https://doi.org/10.1113/jphysiol.2012.247817.
Isaksen, T.J., Kros, L., Vedovato, N., Holm, T.H., Vitenzon, A., Gadsby, D.C., Khodakhah, K., Lykke-Hartmann, K., 2017. Hypothermia-induced dystonia and abnormal cerebellar activity in a mouse model with a single disease-mutation in the sodium-potassium pump. PLoS Genet. 13. https://doi.org/10.1371/journal.pgen.1006763.
Ishii, A., Saito, Y., Mitsui, J., Ishiura, H., Yoshimura, J., Arai, H., Yamashita, S., Kimura, S., Oguni, H., Morishita, S., Tsuji, S., Sasaki, M., Hirose, S., 2013. Identification of ATP1A3 mutations by exome sequencing as the cause of alternating hemiplegia of childhood in Japanese patients. PloS One 8. https://doi.org/10.1371/journal.pone.0056120.

Ishimura, R., Nagy, G., Dotu, I., Chuang, J.H., Ackerman, S.L., 2016. Activation of GCN2 kinase by ribosome stalling links translation elongation with translation initiation. Elife 5, 1–22. https://doi.org/10.7554/eLife.14295.

Jaffer, F., Avbersek, A., Vavassori, R., Fons, C., Campistol, J., Stagnaro, M., De Grandis, E., Veneselli, E., Rosewich, H., Gianotta, M., Zucca, C., Ragona, F., Granata, T., Nardocci, N., Mikati, M., Helseth, A.R., Boelman, C., Minassian, B.A., Johns, S., Garry, S.I., Scheffer, I.E., Gourfinkel-An, I., Carrilho, I., Aylett, S.E., Parton, M., Hanna, M.G., Houlden, H., Neville, B., Kurian, M.A., Novy, J., Sander, J. W., Lambiase, P.D., Behr, E.R., Schyns, T., Arzimanoglou, A., Cross, J.H., Kaski, J.P., Sisodiya, S.M., 2015. Faulty cardiac repolarization reserve in alternating hemiplegia of childhood broadens the phenotype. Brain 138, 2859–2874. https://doi.org/10.1093/brain/awv243.

Jankowsky, J.L., Fadale, D.J., Anderson, J., Xu, G.M., Gonzales, V., Jenkins, N.A., Copeland, N.G., Lee, M.K., Younkin, L.H., Wagner, S.L., Younkin, S.G., Borchelt, D. R., 2004. Mutant presenilins specifically elevate the levels of the 42 residue β-amyloid peptide in vivo: evidence for augmentation of a 42-specific γ secretase. Hum. Mol. Genet. 13, 159–170. https://doi.org/10.1093/hmg/ddh019.

Jansen, N.A., Perez, C., Schenke, M., van Beurden, A.W., Dehghani, A., Voskuyl, R.A., Thijs, R.D., Ullah, G., van den Maagdenberg, A.M.J.M., Tolner, E.A., 2021. Impaired θ-γ coupling indicates inhibitory dysfunction and seizure risk in a Dravet syndrome mouse model. J. Neurosci. 41, 524–537. https://doi.org/10.1523/JNEUROSCI.2132-20.2020.

Jeffery, C.J., 2020. Enzymes, pseudoenzymes, and moonlighting proteins: diversity of function in protein superfamilies. FEBS J. 287, 4141–4149. https://doi.org/10.1111/febs.15446.

Jiao, S., Johnson, K., Moreno, C., Yano, S., Holmgren, M., 2022. Comparative description of the mRNA expression profile of Na+/K+-ATPase isoforms in adult mouse nervous system. J. Comp. Neurol. 530, 627–647. https://doi.org/10.1002/cne.25234.

Jing, X., Wang, L., Song, M., Geng, H., Li, W., Huo, Y., Huang, A., Wang, X., An, C., 2024. Serum neurofilament light chain and inflammatory cytokines as biomarkers for early detection of mild cognitive impairment. Sci. Rep. 14, 1–10. https://doi.org/10.1038/s41598-024-59530-5.

Jinnah, H.A., Neychev, V., Hess, E.J., 2017. The anatomical basis for dystonia: the motor network model. Tremor Other Hyperkinet. Mov. (N. Y) 7, 506. https://doi.org/10.7916/D8V69X3S.

Jung, Y., Damoiseaux, J.S., 2023. The potential of blood neurofilament light as a marker of neurodegeneration for Alzheimer's disease. Brain 147, 12–25. https://doi.org/10.1093/brain/awad267.

Kalotay, E., Klugmann, M., Housley, G.D., Fröhlich, D., 2023. Dominant aminoacyl-tRNA synthetase disorders: lessons learned from in vivo disease models. Front. Neurosci. 17. https://doi.org/10.3389/fnins.2023.1182845.

Kirschen, M.P., Yehya, N., Graham, K., Kilbaugh, T., Berg, R.A., Topjian, A., Diaz-Arrastia, R., 2020. Circulating Neurofilament Light chain is associated with survival after pediatric cardiac arrest. Pediatr. Crit. Care Med. A J. Soc. Crit. Care Med. World Fed. Pediatr. Intensive Crit. Care Soc. 21, 656–661. https://doi.org/10.1097/PCC.0000000000002294.

Kogan, E., Lu, J., Zuo, Y., 2023. Cortical circuit dynamics underlying motor skill learning: from rodents to humans. Front. Mol. Neurosci. 16. https://doi.org/10.3389/fnmol.2023.1292685.

Kropotov, J.D., 2009. Chapter 4 - frontal midline Theta rhythm. In: Kropotov, J.D. (Ed.), Quantitative EEG, Event-Related Potentials and Neurotherapy. Academic Press, San Diego, pp. 77–95. https://doi.org/10.1016/B978-0-12-374512-5.00004-9.

Kros, L., Eelkman Rooda, O.H.J., Spanke, J.K., Alva, P., van Dongen, M.N., Karapatis, A., Tolner, E.A., Strydis, C., Davey, N., Winkelman, B.H.J., Negrello, M., Serdijn, W.A., Steuber, V., van den Maagdenberg, A.M.J.M., De Zeeuw, C.I., Hoebeek, F.E., 2015. Cerebellar output controls generalized spike-and-wave discharge occurrence. Ann. Neurol. 77, 1027–1049. https://doi.org/10.1002/ana.24399.

Lazarov, E., Hillebrand, M., Schröder, S., Ternka, K., Hofhuis, J., Ohlenbusch, A., Barrantes-Freer, A., Pardo, L.A., Fruergaard, M.U., Nissen, P., Brockmann, K., Gärtner, J., Rosewich, H., 2020. Comparative analysis of alternating hemiplegia of childhood and rapid-onset dystonia-parkinsonism ATP1A3 mutations reveals functional deficits, which do not correlate with disease severity. Neurobiol. Dis. 143, 105012. https://doi.org/10.1016/j.nbd.2020.105012.

Letts, V.A., Beyer, B.J., Frankel, W.N., 2014. Hidden in plain sight: spike-wave discharges in mouse inbred strains. Genes Brain Behav. 13, 519–526. https://doi.org/10.1111/gbb.12142.

Levin, S.I., Khaliq, Z.M., Aman, T.K., Grieco, T.M., Kearney, J.A., Raman, I.M., Meisler, M.H., 2006. Impaired motor function in mice with cell-specific knockout of sodium channel Scn8a (NaV1.6) in cerebellar Purkinje neurons and granule cells. J. Neurophysiol. 96, 785–793. https://doi.org/10.1152/jn.01193.2005.

Li, M., Jazayeri, D., Corry, B., McSweeney, K.M., Heinzen, E.L., Goldstein, D.B., Petrou, S., 2015. A functional correlate of severity in alternating hemiplegia of childhood. Neurobiol. Dis. 77, 88–93. https://doi.org/10.1016/j.nbd.2015.02.002.

Li, Y., Liu, X., Wang, C., Su, Z., Zhao, K., Yang, M., Chen, S., Zhou, L., 2022. Molecular and clinical characteristics of ATP1A3-related diseases. Front. Neurol. 13. https://doi.org/10.3389/fneur.2022.924788.

Linder, C.C., Davission, T.M., 2004. Strains, stocks, and mutant mice. Lab. Mouse. Acad. Press Chapter 3, 25–46.

Liu, M., Jiang, L., Wen, M., Ke, Y., Tong, X., Huang, W., Chen, R., 2020. Microglia depletion exacerbates acute seizures and hippocampal neuronal degeneration in mouse models of epilepsy. Am. J. Physiol. - Cell Physiol. 319, C605–C610. https://doi.org/10.1152/ajpcell.00205.2020.

Liu, Y.B., Arystarkhova, E., Sacino, A.N., Szabari, M.V., Lutz, C.M., Terrey, M., Morsci, N., Jakobs, T.C., Lykke-Hartmann, K., Brashear, A., Napoli, E., Sweadner, K. J., 2024. Phenotype distinctions in mice deficient in the neuron-specific α3 subunit of Na,K-ATPase: Atp1a3^{tm1Ling/+}and Atp1a3^{+/D801Y} eneuro ENEURO.0101–24.2024. https://doi.org/10.1523/ENEURO.0101-24.2024.

Livak, K.J., Schmittgen, T.D., 2001. Analysis of relative gene expression data using real-time quantitative PCR and the 2-ΔΔCT method. Methods 25, 402–408. https://doi.org/10.1006/meth.2001.1262.

Loher, T.J., Krauss, J.K., 2009. Dystonia associated with pontomesencephalic lesions. Mov. Disord. 24, 157–167. https://doi.org/10.1002/mds.22196.

Loonen, I.C.M., Jansen, N.A., Cain, S.M., Schenke, M., Voskuyl, R.A., Yung, A.C., Bohnet, B., Kozlowski, P., Thijs, R.D., Ferrari, M.D., Snutch, T.P., van den Maagdenberg, A.M.J.M., Tolner, E.A., 2019. Brainstem spreading depolarization and cortical dynamics during fatal seizures in Cacna1a S218L mice. Brain 142, 412–425. https://doi.org/10.1093/brain/awy325.

Loreaux, E.L., Kaul, B., Lorenz, J.N., Lingrel, J.B., 2008. Ouabain-Sensitive alpha1 Na,K-ATPase enhances natriuretic response to saline load. J. Am. Soc. Nephrol. 19, 1947–1954. https://doi.org/10.1681/ASN.2008020174.

Love, M.I., Huber, W., Anders, S., 2014. Moderated estimation of fold change and dispersion for RNA-seq data with DESeq2. Genome Biol. 15, 1–21. https://doi.org/10.1186/s13059-014-0550-8.

Luo, H., Huang, X., Li, Z., Tian, W., Fang, K., Liu, T., Wang, S., Tang, B., Hu, J., Yuan, T.-F., Cao, L., 2024. An electroencephalography profile of paroxysmal Kinesigenic dyskinesia. Adv. Sci. (Weinheim, Baden-Wurttemberg, Ger.) 11, e2306321. https://doi.org/10.1002/advs.202306321.

Martin, M., 2011. Cutadapt removes adapter sequences from high-throughput sequencing reads. EMBnet.journal 17, 10–12. https://doi.org/10.14806/ej.17.1.200.

McGrail, K.M., Phillips, J.M., Sweadner, K.J., 1991. Immunofluorescent localization of three Na,K-ATPase isozymes in the rat central nervous system: Both neurons and glia can Express more than one Na. K-ATPase. J. Neurosci. 11, 381–391. https://doi.org/10.1523/jneurosci.11-02-00381.1991.

McLellan, M.A., Skelly, D.A., Dona, M.S.I., Squiers, G.T., Farrugia, G.E., Gaynor, T.L., Cohen, C.D., Pandey, R., Diep, H., Vinh, A., Rosenthal, N.A., Pinto, A.R., 2020. High-resolution transcriptomic profiling of the heart during chronic stress reveals cellular drivers of cardiac fibrosis and hypertrophy. Circulation 142, 1448–1463. https://doi.org/10.1161/CIRCULATIONAHA.119.045115.

Minkeviciene, R., Rheims, S., Dobszay, M.B., Zilberter, M., Hartikainen, J., Fülöp, L., Penke, B., Zilberter, Y., Harkany, T., Pitkänen, A., Tanila, H., 2009. Amyloid β-induced neuronal hyperexcitability triggers progressive epilepsy. J. Neurosci. 29, 3453–3462. https://doi.org/10.1523/JNEUROSCI.5215-08.2009.

Moseley, A.E., Williams, M.T., Schaefer, T.L., Bohanan, C.S., Neumann, J.C., Behbehani, M.M., Vorhees, C.V., Lingrel, J.B., 2007. Deficiency in Na,K-ATPase α isoform genes alters spatial learning, motor activity, and anxiety in mice. J. Neurosci. 27, 616–626. https://doi.org/10.1523/JNEUROSCI.4464-06.2007.

Motelow, J.E., Blumenfeld, H., 2009. Functional neuroimaging of spike-wave seizures. Methods Mol. Biol. 489, 189–209. https://doi.org/10.1007/978-1-59745-543-5_9.

Moya-Mendez, M.E., Ogbonna, C., Ezekian, J.E., Rosamilia, M.B., Prange, L., de la Uz, C., Kim, J.J., Howard, T., Garcia, J., Nussbaum, R., Truty, R., Callis, T.E., Funk, E., Heyes, M., de Dear, G.L., Carboni, M.P., Idriss, S.F., Mikati, M.A., Landstrom, A.P., 2021. Atp1a3-encoded sodium-potassium atpase subunit alpha 3 d801n variant is associated with shortened qt interval and predisposition to ventricular fibrillation preceded by bradycardia. J. Am. Heart Assoc. 10. https://doi.org/10.1161/JAHA.120.019887.

Mueller, S.G., Bateman, L.M., Nei, M., Goldman, A.M., Laxer, K.D., 2019. Brainstem atrophy in focal epilepsy destabilizes brainstem-brain interactions: preliminary findings. NeuroImage Clin. 23. https://doi.org/10.1016/j.nicl.2019.101888.

Neville, B.G.R., Ninan, M., 2007. The treatment and management of alternating hemiplegia of childhood. Dev. Med. Child Neurol. 49, 777–780. https://doi.org/10.1111/j.1469-8749.2007.00777.x.

Neychev, V.K., Fan, X., Mitev, V.I., Hess, E.J., Jinnah, H.A., 2008. The basal ganglia and cerebellum interact in the expression of dystonic movement. Brain 131, 2499–2509. https://doi.org/10.1093/brain/awn168.

Ng, H.W.Y., Ogbeta, J.A., Clapcote, S.J., 2021. Genetically altered animal models for ATP1A3-related disorders. DMM Dis. Model. Mech. 14. https://doi.org/10.1242/dmm.048938.

Nguyen, A.D., Malmstrom, T.K., Aggarwal, G., Miller, D.K., Vellas, B., Morley, J.E., 2022. Serum neurofilament light levels are predictive of all-cause mortality in late middle-aged individuals. eBioMedicine 82, 104146. https://doi.org/10.1016/j.ebiom.2022.104146.

O'Brien, W.J., Lingrel, J.B., Wallick, E.T., 1994. Ouabain binding kinetics of the rat alpha two and alpha three isoforms of the sodium-potassium adenosine triphosphate. Arch. Biochem. Biophys. 310, 32–39. https://doi.org/10.1006/abbi.1994.1136.

Oestereicher, M.A., Wotton, J.M., Ayabe, S., Bou About, G., Cheng, T.K., Choi, J.-H., Clary, D., Dew, E.M., Elfertak, L., Guimond, A., Haseli Mashhadi, H., Heaney, J.D., Kelsey, L., Keskivali-Bond, P., Lopez Gomez, F., Marschall, S., McFarland, M., Meziane, H., Munoz Fuentes, V., Nam, K.-H., Nichtová, Z., Pimm, D., Bower, L., Prochazka, J., Rozman, J., Santos, L., Stewart, M., Tanaka, N., Ward, C.S., Willett, A. M.E., Wilson, R., Braun, R.E., Dickinson, M.E., Flenniken, A.M., Herault, Y., Lloyd, K. C.K., Mallon, A.-M., McKerlie, C., Murray, S.A., Nutter, L.M.J., Sedlacek, R., Seong, J. K., Sorg, T., Tamura, M., Wells, S., Schneltzer, E., Fuchs, H., Gailus-Durner, V., Hrabe de Angelis, M., White, J.K., Spielmann, N., 2023. Comprehensive ECG reference intervals in C57BL/6N substrains provide a generalizable guide for cardiac electrophysiology studies in mice. Mamm. Genome 34, 180–199. https://doi.org/10.1007/s00335-023-09995-y.

Orre, M., Kamphuis, W., Osborn, L.M., Jansen, A.H.P., Kooijman, L., Bossers, K., Hol, E. M., 2014. Isolation of glia from Alzheimer's mice reveals inflammation and dysfunction. Neurobiol. Aging 35, 2746–2760. https://doi.org/10.1016/j.neurobiolaging.2014.06.004.

Paciorkowski, A.R., McDaniel, S.S., Jansen, L.A., Tully, H., Tuttle, E., Ghoneim, D.H., Tupal, S., Gunter, S.A., Vasta, V., Zhang, Q., Tran, T., Liu, Y.B., Ozelius, L.J., Brashear, A., Sweadner, K.J., Dobyns, W.B., Hahn, S., 2015. Novel mutations in ATP1A3 associated with catastrophic early life epilepsy, episodic prolonged apnea, and postnatal microcephaly. Epilepsia 56, 422–430. https://doi.org/10.1111/epi.12914.

Palmgren, M.G., Nissen, P., 2011. P-type ATPases. Annu. Rev. Biophys. 40, 243–266. https://doi.org/10.1146/annurev.biophys.093008.131331.

Pan, C., Li, B., Simon, M.C., 2021. Moonlighting functions of metabolic enzymes and metabolites in cancer. Mol. Cell 81, 3760–3774. https://doi.org/10.1016/j.molcel.2021.08.031.

Panagiotakaki, E., Gobbi, G., Neville, B., Ebinger, F., Campistol, J., Nevšímalová, S., Laan, L., Casaer, P., Spiel, G., Giannotta, M., Fons, C., Ninan, M., Sange, G., Schyns, T., Vavassori, R., Poncelin, D., Arzimanoglou, A., 2010. Evidence of a non-progressive course of alternating hemiplegia of childhood: study of a large cohort of children and adults. Brain 133, 3598–3610. https://doi.org/10.1093/brain/awq295.

Panagiotakaki, Eleni, de Grandis, E., Stagnaro, M., Heinzen, E.L., Fons, C., Sisodiya, S., De Vries, B., Goubau, C., Weckhuysen, S., Kemlink, D., Scheffer, I., Lesca, G., Rabilloud, Muriel, Klich, A., Ramirez-Camacho, A., Ulate-Campos, A., Campistol, J., Giannotta, M., Moutard, Marie Laure, Doummar, Diane, Hubsch-Bonneaud, Cecile, Jaffer, F., Cross, H., Gurrieri, F., Tiziano, D., Nevsimalova, S., Nicole, Sophie, Neville, B., van den Maagdenberg, A.M.J.M., Mikati, M., Goldstein, D.B., Vavassori, R., Arzimanoglou, Alexis, Bassi, M.T., Borgatti, R., Cernetti, R., Di Rosa, G., Franchini, F., Gambardella, A., Giacanelli, M., Gobbi, G., Granata, T., Guerrini, R., Incorpora, G., Nardocci, N., Neri, G., Ragona, F., Santucci, M., Sartori, S., Veneselli, E., Vigevano, F., Zucca, C., Aicardi, J., An, I., Arbues, A.S., Arzimanoglou, A., Bahi-Buisson, N., Barthez, M.A., Billette de Villemeur, T., Bourgeois, M., Bru, M., Chabrol, B., Chaigne, D., Chaunu, M.P., Chaunu, C., Cournelle, A.M., Davoine, C.S., De St Martin, A., Deny, B., Desguerres, I., Des Portes, V., Doummar, D., Dulac, O., Dusser, A., Gerard, M., Gitiaux, C., Godet Kiesel, I., Gokben, S., Goutieres, F., Guerrin, M.H., Heron-Longe, B., Hubsch-Bonneaud, C., Hully, M., Husson, M., Husson, C., Kaminska, A., Laroche, C., Lazaro, L., Lepine, A., Magy, L., Marchal, C., Michel, J., Milh, M., Motte, J., Moutard, M.L., Napuri, S., Nassogne, M.C., Neau, J.P., Nicole, S., Panagiotakaki, E., Passemard, S., Pedespan, J.M., Penniello-Valette, M.J., Poncelin, D., Ponsot, G., Poulat, A.L., Pouplard, F., Rabilloud, M., Riant, F., Rivier, F., Roelens, P., Roubergue, A., Sanlaville, D., Tardieu, M., Veyrieres, S., de Jonghe, P., Goubeau, C., Krepelova, A., Kolnikova, M., Sykora, P., Kaski, J., Hanna, M., Houlden, H., Cancho, R., Eiris, J., López-Laso, E., Velázquez, R., Carilho, I., Ozelius, L., Suls, A., Ceulemans, B., Buyse, G., di Michele, M., Ferrari, M., Peeters-Scholte, C.M.P.C.D., 2015. Clinical profile of patients with ATP1A3 mutations in alternating hemiplegia of childhood - a study of 155 patients. Orphanet J. Rare Dis. 10. https://doi.org/10.1186/s13023-015-0335-5.

Pass, R., Haan, N., Humby, T., Wilkinson, L.S., Hall, J., Thomas, K.L., 2022. Selective behavioural impairments in mice heterozygous for the cross disorder psychiatric risk gene DLG2. Genes Brain Behav. 21, 1–13. https://doi.org/10.1111/gbb.12799.

Pavone, P., Pappalardo, X.G., Mustafa, N., Cho, S.Y., Jin, D.K., Incorpora, G., Falsaperla, R., Marino, S.D., Corsello, G., Parano, E., Ruggieri, M., 2022a. Alternating hemiplegia of childhood: neurological comorbidities and intrafamilial variability. Ital. J. Pediatr. 48, 1–11. https://doi.org/10.1186/s13052-021-01194-2.

Pavone, P., Pappalardo, X.G., Ruggieri, M., Falsaperla, R., Parano, E., 2022b. Alternating hemiplegia of childhood: a distinct clinical entity and ATP1A3-related disorders: a narrative review. Med. (United States) 101, E29413. https://doi.org/10.1097/MD.0000000000029413.

Perez, V., Duque, A., Hidalgo, V., Salvador, A., 2024. EEG frequency bands in subjective cognitive decline: a systematic review of resting state studies. Biol. Psychol. 191, 108823. https://doi.org/10.1016/j.biopsycho.2024.108823.

Perulli, M., Poole, J., Di Lazzaro, G., D'Ambrosio, S., Silvennoinen, K., Zagaglia, S., Jiménez-Jiménez, D., Battaglia, D., Sisodiya, S.M., Balestrini, S., 2022. Non-stationary outcome of alternating hemiplegia of childhood into adulthood. Mov. Disord. Clin. Pract. 9, 206–211. https://doi.org/10.1002/mdc3.13388.

Pizoli, C.E., Jinnah, H.A., Billingsley, M.L., Hess, E.J., 2002. Abnormal cerebellar signaling induces dystonia in mice. J. Neurosci. 22, 7825–7833. https://doi.org/10.1523/jneurosci.22-17-07825.2002.

Polanowska, K.E., Dzieżyc, K., Rosewich, H., Ohlenbusch, A., Seniów, J.B., 2018. Alternating Hemiplegia of Childhood in Two Adult Patients with a Mild Syndrome. Cogn. Behav. Neurol. 31.

Pracucci, E., Pillai, V., Lamers, D., Parra, R., Landi, S., 2021. Neuroinflammation: a signature or a cause of epilepsy? Int. J. Mol. Sci. 22, 1–18. https://doi.org/10.3390/ijms22136981.

Premont, A., Saadeh, K., Edling, C., Lewis, R., Marr, C.M., Jeevaratnam, K., 2022. Cardiac ion channel expression in the equine model - in-silico prediction utilising RNA sequencing data from mixed tissue samples. Physiol. Rep. 10, e15273. https://doi.org/10.14814/phy2.15273.

Price, E.M., Lingrel, J.B., 1988. Structure-function relationships in the Na,K-ATPase alpha subunit: site-directed mutagenesis of glutamine-111 to arginine and asparagine-122 to aspartic acid generates a ouabain-resistant enzyme. Biochemistry 27, 8400–8408. https://doi.org/10.1021/bi00422a016.

Racine, R.J., 1972. Modification of seizure activity by electrical stimulation. II. Motor seizure. Electroencephalogr. Clin. Neurophysiol. 32, 281–294. https://doi.org/10.1016/0013-4694(72)90177-0.

Radu, B.M., Epureanu, F.B., Radu, M., Fabene, P.F., Bertini, G., 2017. Nonsteroidal anti-inflammatory drugs in clinical and experimental epilepsy. Epilepsy Res. 131, 15–27. https://doi.org/10.1016/j.eplepsyres.2017.02.003.

Rosewich, H., Thiele, H., Ohlenbusch, A., Maschke, U., Altmüller, J., Frommolt, P., Zirn, B., Ebinger, F., Siemes, H., Nürnberg, P., Brockmann, K., Gärtner, J., 2012. Heterozygous de-novo mutations in ATP1A3 in patients with alternating hemiplegia of childhood: a whole-exome sequencing gene-identification study. Lancet Neurol. 11, 764–773. https://doi.org/10.1016/S1474-4422(12)70182-5.

Sabouraud, P., Riquet, A., Spitz, M.A., Deiva, K., Nevsimalova, S., Mignot, C., Lesca, G., Bednarek, N., Doummar, D., Pietrement, C., Laugel, V., 2019. Relapsing encephalopathy with cerebellar ataxia are caused by variants involving p.Arg756 in ATP1A3. Eur. J. Paediatr. Neurol. 23, 448–455. https://doi.org/10.1016/j.ejpn.2019.02.004.

Saito, Y., Inui, T., Sakakibara, T., Sugai, K., Sakuma, H., Sasaki, M., 2010. Evolution of hemiplegic attacks and epileptic seizures in alternating hemiplegia of childhood. Epilepsy Res. 90, 248–258. https://doi.org/10.1016/j.eplepsyres.2010.05.013.

Salles, P.A., Mata, I.F., Brünger, T., Lal, D., Fernandez, H.H., 2021. ATP1A3-related disorders: An ever-expanding clinical Spectrum. Front. Neurol. 12, 1–13. https://doi.org/10.3389/fneur.2021.637890.

Sanz, P., Rubio, T., Garcia-Gimeno, M.A., 2024. Neuroinflammation and epilepsy: from pathophysiology to therapies based on repurposing drugs. Int. J. Mol. Sci. 25. https://doi.org/10.3390/ijms25084161.

Sasaki, M., Ishii, A., Saito, Y., Morisada, N., Iijima, K., Takada, S., Araki, A., Tanabe, Y., Arai, H., Yamashita, S., Ohashi, T., Oda, Y., Ichiseki, H., Hirabayashi, S., Yasuhara, A., Kawawaki, H., Kimura, S., Shimono, M., Narumiya, S., Suzuki, M., Yoshida, T., Oyazato, Y., Tsuneishi, S., Ozasa, S., Yokochi, K., Dejima, S., Akiyama, T., Kishi, N., Kira, R., Ikeda, T., Oguni, H., Zhang, B., Tsuji, S., Hirose, S., 2014. Genotype-phenotype correlations in alternating hemiplegia of childhood. Neurology 82, 482–490. https://doi.org/10.1212/WNL.0000000000000102.

Sasaki, M., Ishii, A., Saito, Y., Hirose, S., 2017. Progressive brain atrophy in alternating hemiplegia of childhood. Mov. Disord. Clin. Pract. 4, 406–411. https://doi.org/10.1002/mdc3.12451.

Seibenhener, M.L., Wooten, M.C., 2015. Use of the open field maze to measure locomotor and anxiety-like behavior in mice. J. Vis. Exp. 1–6. https://doi.org/10.3791/52434.

Seidler, R.D., 2010. Neural correlates of motor learning, transfer of learning, and learning to learn. Exerc. Sport Sci. Rev. 38, 3–9. https://doi.org/10.1097/JES.0b013e3181c5cce7.

Selman, C., Swindell, W.R., 2018. Putting a strain on diversity. EMBO J. 37, 1–6. https://doi.org/10.15252/embj.2018100862.

Shamraj, O.I., Melvin, D., Lingrel, J.B., 1991. Expression of Na,K-ATPase isoforms in human heart. Biochem. Biophys. Res. Commun. 179, 1434–1440. https://doi.org/10.1016/0006-291x(91)91733-s.

Simmons, C.Q., Thompson, C.H., Cawthon, B.E., Westlake, G., Swoboda, K.J., Kiskinis, E., Ess, K.C., George, A.L., 2018. Direct evidence of impaired neuronal Na/K-ATPase pump function in alternating hemiplegia of childhood. Neurobiol. Dis. 115, 29–38. https://doi.org/10.1016/j.nbd.2018.03.009.

Smith, R.S., Florio, M., Akula, S.K., Neil, J.E., Wang, Y., Sean Hill, R., Goldman, M., Mullally, C.D., Reed, N., Bello-Espinosa, L., Flores-Sarnat, L., Monteiro, F.P., Erasmo, C.B., Vairo, F.P.E., Morava, E., James Barkovich, A., Gonzalez-Heydrich, J., Brownstein, C.A., McCarroll, S.A., Walsh, C.A., 2021. Early role for a Na+,K+-ATPase (ATP1A3) in brain development. Proc. Natl. Acad. Sci. U. S. A. 118, 1–11. https://doi.org/10.1073/pnas.2023333118.

Snaebjornsson, M.T., Schulze, A., 2018. Non-canonical functions of enzymes facilitate cross-talk between cell metabolic and regulatory pathways. Exp. Mol. Med. 50. https://doi.org/10.1038/s12276-018-0065-6.

Soneson, C., Love, M.I., Robinson, M.D., 2015. Differential analyses for RNA-seq: transcript-level estimates improve gene-level inferences. F1000Research 4, 1521. https://doi.org/10.12688/f1000research.7563.1.

Stephens, M., 2017. False discovery rates: a new deal. Biostatistics 18, 275–294. https://doi.org/10.1093/biostatistics/kxw041.

Suleymanova, E.M., 2021. Behavioral comorbidities of epilepsy and neuroinflammation: evidence from experimental and clinical studies. Epilepsy Behav. 117, 107869. https://doi.org/10.1016/j.yebeh.2021.107869.

Sun, L., Wei, N., Kuhle, B., Blocquel, D., Novick, S., Matuszek, Z., Zhou, H., He, W., Zhang, J., Weber, T., Horvath, R., Latour, P., Pan, T., Schimmel, P., Griffin, P.R., Yang, X.L., 2021. CMT2N-causing aminoacylation domain mutants enable Nrp1 interaction with AlaRS. Proc. Natl. Acad. Sci. U. S. A. 118, 1–9. https://doi.org/10.1073/pnas.2012898118.

Sweadner, K.J., 2016. Colorimetric Assays of Na,K-ATPase. Methods Mol. Biol. 1377, 89–104. https://doi.org/10.1007/978-1-4939-3179-8_10.

Sweadner, K.J., Herrera, V.L., Amato, S., Moellmann, A., Gibbons, D.K., Repke, K.R., 1994. Immunologic identification of Na+,K(+)-ATPase isoforms in myocardium. Isoform change in deoxycorticosterone acetate-salt hypertension. Circ. Res. 74, 669–678. https://doi.org/10.1161/01.res.74.4.669.

Sweadner, K.J., Arystarkhova, E., Penniston, J.T., Swoboda, K.J., Brashear, A., Ozelius, L.J., 2019. Genotype-structure-phenotype relationships diverge in paralogs ATP1A1, ATP1A2, and ATP1A3. Neurol. Genet. 5. https://doi.org/10.1212/NXG.0000000000000303.

Sweney, M.T., Newcomb, T.M., Swoboda, K.J., 2015. The expanding spectrum of neurological phenotypes in children with ATP1A3 mutations, alternating hemiplegia of childhood, rapid-onset dystonia-parkinsonism, CAPOS and beyond. Pediatr. Neurol. 52, 56–64. https://doi.org/10.1016/j.pediatrneurol.2014.09.015.

Syeda, S.S., Sánchez, G., McDermott, J.P., Hong, K.H., Blanco, G., Georg, G.I., 2020. The Na+ and K+ transport system of sperm (ATP1A4) is essential for male fertility and an attractive target for male contraception. Biol. Reprod. 103, 343–356. https://doi.org/10.1093/biolre/ioaa093.

Tamim, I., Chung, D.Y., de Morais, A.L., Loonen, I.C.M., Qin, T., Misra, A., Schlunk, F., Endres, M., Schiff, S.J., Ayata, C., 2021. Spreading depression as an innate antiseizure mechanism. Nat. Commun. 12, 2206. https://doi.org/10.1038/s41467-021-22464-x.

Tan, E., Troller-Renfree, S.V., Morales, S., Buzzell, G.A., McSweeney, M., Antúnez, M., Fox, N.A., 2024. Theta activity and cognitive functioning: integrating evidence from resting-state and task-related developmental electroencephalography (EEG) research. Dev. Cogn. Neurosci. 67, 101404. https://doi.org/10.1016/j.dcn.2024.101404.

Tatem, K.S., Quinn, J.L., Phadke, A., Yu, Q., Gordish-Dressman, H., Nagaraju, K., 2014. Behavioral and locomotor measurements using an open field activity monitoring system for skeletal muscle diseases. J. Vis. Exp. 1–7. https://doi.org/10.3791/51785.

Tivadar, R.I., Murray, M.M., 2019. A primer on electroencephalography and event-related potentials for organizational neuroscience. Organ. Res. Methods 22, 69–94. https://doi.org/10.1177/1094428118804657.

Tokuda, S., Beyer, B.J., Frankel, W.N., 2009. Genetic complexity of absence seizures in substrains of C3H mice. Genes Brain Behav. 8, 283–289. https://doi.org/10.1111/j.1601-183X.2008.00472.x.

Tranebjærg, L., Strenzke, N., Lindholm, S., Rendtorff, N.D., Poulsen, H., Khandelia, H., Kopec, W., Lyngbye, T.J.B., Hamel, C., Delettre, C., Bocquet, B., Bille, M., Owen, H. H., Bek, T., Jensen, H., Østergaard, K., Möller, C., Luxon, L., Carr, L., Wilson, L., Rajput, K., Sirimanna, T., Harrop-Griffiths, K., Rahman, S., Vona, B., Doll, J., Haaf, T., Bartsch, O., Rosewich, H., Moser, T., Bitner-Glindzicz, M., 2018. The CAPOS mutation in ATP1A3 alters Na/K-ATPase function and results in auditory neuropathy which has implications for management. Hum. Genet. 137, 111–127. https://doi.org/10.1007/s00439-017-1862-z.

Uchitel, J., Abdelnour, E., Boggs, A., Prange, L., Pratt, M., Bonner, M., Jasien, J., Dawson, G., Abrahamsen, T., Mikati, M.A., 2020. Social impairments in alternating hemiplegia of childhood. Dev. Med. Child Neurol. 62, 820–826. https://doi.org/10.1111/dmcn.14473.

Uchitel, J., Wallace, K., Tran, L., Abrahamsen, T., Hunanyan, A., Prange, L., Jasien, J., Caligiuri, L., Pratt, M., Rikard, B., Fons, C., De Grandis, E., Vezyroglou, A., Heinzen, E.L., Goldstein, D.B., Vavassori, R., Papadopoulou, M.T., Cocco, I., Moré, R., Arzimanoglou, A., Panagiotakaki, E., Mikati, M.A., 2021. Alternating hemiplegia of childhood: evolution over time and mouse model corroboration. Brain Commun. 3, 1–17. https://doi.org/10.1093/braincomms/fcab128.

Uher, T., McComb, M., Galkin, S., Srpova, B., Oechtering, J., Barro, C., Tyblova, M., Bergsland, N., Krasensky, J., Dwyer, M., Havrdova, E.K., Posova, H., Vaneckova, M., Zivadinov, R., Horakova, D., Kuhle, J., Ramanathan, M., 2021. Neurofilament levels are associated with blood–brain barrier integrity, lymphocyte extravasation, and risk factors following the first demyelinating event in multiple sclerosis. Mult. Scler. J. 27, 220–231. https://doi.org/10.1177/1352458520912379.

Van Den Bosch, A., Fransen, N., Mason, M., Rozemuller, A.J., Teunissen, C., Smolders, J., Huitinga, I., 2022. Neurofilament Light chain levels in multiple sclerosis correlate with lesions containing foamy macrophages and with acute axonal damage. Neurol. Neuroimmunol. NeuroInflammation 9, 1–11. https://doi.org/10.1212/NXI.0000000000001154.

Van Der Heijden, M.E., Gill, J.S., Rey Hipolito, A.G., Salazar Leon, L.E., Sillitoe, R.V., 2022. Quantification of behavioral deficits in developing mice with dystonic behaviors. Dystonia 1, 1–10. https://doi.org/10.3389/dyst.2022.10494.

Verslegers, M., Van Hove, I., Dekeyster, E., Gantois, I., Hu, T.-T., D'Hooge, R., Arckens, L., Moons, L., 2015. MMP-2 mediates Purkinje cell morphogenesis and spine development in the mouse cerebellum. Brain Struct. Funct. 220, 1601–1617. https://doi.org/10.1007/s00429-014-0747-3.

Vezyroglou, A., Akilapa, R., Barwick, K., Koene, S., Brownstein, C.A., Holder-Espinasse, M., Fry, A.E., Németh, A.H., Tofaris, G.K., Hay, E., Hughes, I., Mansour, S., Mordekar, S.R., Splitt, M., Turnpenny, P.D., Demetriou, D., Koopmann, T.T., Ruivenkamp, C.A.L., Agrawal, P.B., Carr, L., Clowes, V., Ghali, N., Holder, S.E., Radley, J., Male, A., Sisodiya, S.M., Kurian, M.A., Cross, J.H., Balasubramanian, M., 2022. The phenotypic continuum of ATP1A3-related disorders. Neurology 99, E1511–E1526. https://doi.org/10.1212/WNL.0000000000200927.

Villasana-Salazar, B., Vezzani, A., 2023. Neuroinflammation microenvironment sharpens seizure circuit. Neurobiol. Dis. 178, 106027. https://doi.org/10.1016/j.nbd.2023.106027.

Viollet, L., Glusman, G., Murphy, K.J., Newcomb, T.M., Reyna, S.P., Sweney, M., Nelson, B., Andermann, F., Andermann, E., Acsadi, G., Barbano, R.L., Brown, C., Brunkow, M.E., Chugani, H.T., Cheyette, S.R., Collins, A., Debrosse, S.D., Galas, D., Friedman, J., Hood, L., Huff, C., Jorde, L.B., King, M.D., Lasalle, B., Leventer, R.J., Lewelt, A.J., Massart, M.B., Mérida, M.R., Ptáček, L.J., Roach, J.C., Rust, R.S., Renault, F., Sanger, T.D., Sotero De Menezes, M.A., Tennyson, R., Uldall, P., Zhang, Y., Zupanc, M., Xin, W., Silver, K., Swoboda, K.J., 2015. Alternating hemiplegia of childhood: retrospective genetic study and genotype-phenotype correlations in 187 subjects from the US AHCF registry. PloS One 10, 25996915. https://doi.org/10.1371/journal.pone.0137370.

Vo, M.N., Terrey, M., Lee, J.W., Roy, B., Moresco, J.J., Sun, L., Fu, H., Liu, Q., Weber, T. G., Yates, J.R., Fredrick, K., Schimmel, P., Ackerman, S.L., 2018. ANKRD16 prevents neuron loss caused by an editing-defective tRNA synthetase. Nature 557, 510–515. https://doi.org/10.1038/s41586-018-0137-8.

Voller, J., Potužáková, B., Šimeček, V., Vožeh, F., 2014. The role of whiskers in compensation of visual deficit in a mouse model of retinal degeneration. Neurosci. Lett. 558, 149–153. https://doi.org/10.1016/j.neulet.2013.11.005.

Wagner, J.M., Sichler, M.E., Schleicher, E.M., Franke, T.N., Irwin, C., Löw, M.J., Beindorff, N., Bouter, C., Bayer, T.A., Bouter, Y., 2019. Analysis of motor function in the Tg4-42 mouse model of alzheimer's disease. Front. Behav. Neurosci. 13, 1–13. https://doi.org/10.3389/fnbeh.2019.00107.

Wang, Y., Wu, T., Tsai, M.C., Rezzonico, M.G., Abdel-Haleem, A.M., Xie, L., Gandham, V. D., Ngu, H., Stark, K., Glock, C., Xu, D., Foreman, O., Friedman, B.A., Sheng, M., Hanson, J.E., 2023. TPL2 kinase activity regulates microglial inflammatory responses and promotes neurodegeneration in tauopathy mice. Elife 12, 1–29. https://doi.org/10.7554/eLife.83451.

Weigand, K.M., Messchaert, M., Swarts, H.G.P., Russel, F.G.M., Koenderink, J.B., 2014. Alternating Hemiplegia of Childhood mutations have a differential effect on Na+,K+-ATPase activity and ouabain binding. Biochim. Biophys. Acta - Mol. Basis Dis. 1842, 1010–1016. https://doi.org/10.1016/j.bbadis.2014.03.002.

Wu, Q., Zhao, C.W., Long, Z., Xiao, B., Feng, L., 2018. Anatomy based networks and topology alteration in seizure-related cognitive outcomes. Front. Neuroanat. 12, 1–11. https://doi.org/10.3389/fnana.2018.00025.

Yang, Y., Mason, A.J., 2017. Hardware efficient automatic thresholding for NEO-based neural spike detection. I.E.E.E. Trans. Biomed. Eng. 64, 826–833. https://doi.org/10.1109/TBME.2016.2580319.

Young, D., Mayer, F., Vidotto, N., Schweizer, T., Berth, R., Abramowski, D., Shimshek, D. R., van der Putten, P.H., Schmid, P., 2013. Mutant huntingtin gene-dose impacts on aggregate deposition, DARPP32 expression and Neuroinflammation in HdhQ150 mice. PloS One 8. https://doi.org/10.1371/journal.pone.0075108.

Yuan, A., Nixon, R.A., 2021. Neurofilament proteins as biomarkers to monitor neurological diseases and the efficacy of therapies. Front. Neurosci. 15. https://doi.org/10.3389/fnins.2021.689938.

Zhao, J., Sun, J., Zheng, Yang, Zheng, Yanrong, Shao, Y., Li, Y., Fei, F., Xu, C., Liu, X., Wang, S., Ruan, Y., Liu, J., Duan, S., Chen, Z., Wang, Y., 2022. Activated astrocytes attenuate neocortical seizures in rodent models through driving Na+-K+-ATPase. Nat. Commun. 13, 1–15. https://doi.org/10.1038/s41467-022-34662-2.

Zhen, Z.-H., Guo, M.-R., Li, H.-M., Guo, O.-Y., Zhen, J.-L., Fu, J., Tan, G.-J., 2021. Normal and abnormal Sharp wave ripples in the hippocampal-entorhinal cortex system: implications for memory consolidation, Alzheimer's disease, and temporal lobe epilepsy. Front. Aging Neurosci. 13, 683483. https://doi.org/10.3389/fnagi.2021.683483.

Zou, S., Lan, Y.L., Gong, Y., Chen, Z., Xu, C., 2023. The role of ATP1A3 gene in epilepsy: we need to know more. Front. Cell. Neurosci. 17. https://doi.org/10.3389/fncel.2023.1143956.